Astrophys Space Sci (2010) 325: 259–275
DOI 10.1007/s10509-009-0175-7

ORIGINAL ARTICLE

Effect of a varying gravitational constant on the SN Ia Hubble diagram, AGN luminosity evolution, and X-ray source counts

Roman Tomaschitz

Received: 13 August 2009 / Accepted: 13 October 2009 / Published online: 14 November 2009

Abstract The impact of a cosmic time evolution of the gravitational constant on SN Ia luminosity and AGN/QSO luminosity functions is studied. The gravitational constant scales linearly with the Hubble parameter, its present-day variation being $\dot{G}_0/G_0 \approx 1.9 \times 10^{-4}\,\mathrm{Gyr}^{-1}$, compatible with current bounds from lunar laser ranging. Distance moduli of Type Ia supernovae are fitted with a cosmic expansion factor derived from temperature variations of planetary paleoclimates, and a luminosity dependence on look-back time proportional to the varying gravitational constant is inferred from the Hubble diagram. A fit is performed to the comoving space density of X-ray-selected active galactic nuclei (AGNs) and optically selected quasars (QSOs) extending to redshifts $z \approx 6$. The initial steep increase of the AGN space density is reproduced by a redshift evolution depending solely on the Hubble parameter as scaling variable. The AGN luminosity scales with the Hubble parameter, and the scaling exponents of the luminosity function, composed of two competing power laws with exponential cutoff, are obtained. Based on the AGN luminosity function, flux-limited X-ray source counts are investigated. The counting functions are derived and put to test by fitting cumulative number counts of soft X-ray point sources compiled from ROSAT, XMM-Newton, and Chandra surveys.

Keywords Cosmic time scaling of Newton's constant · Robertson–Walker cosmology · Hubble diagram of Type Ia supernovae · Active galactic nuclei · Luminosity function and comoving space density · Number counts of X-ray point sources

PACS 98.80.Es · 98.62.Py · 98.62.Ve · 95.30.Sf

R. Tomaschitz (✉)
Department of Physics, Hiroshima University, 1-3-1 Kagami-yama, Higashi-Hiroshima 739-8526, Japan
e-mail: tom@geminga.org

1 Introduction

We study a cosmic time scaling of Newton's constant proportional to the Hubble parameter, $G \propto H(z)$, based on the constancy of the moderate dimensionless ratio $\hbar^2 H_0/(G_0 c m_\pi^3)$ where m_π stands for the pion mass. The context is an open Robertson–Walker cosmology with an expansion factor capable of explaining the "faint young sun paradox" (Newman and Rood 1977; Kasting and Catling 2003; Tomaschitz 2005) and resulting in a very small present-day variation $\dot{H}_0/H_0 = \dot{G}_0/G_0 \approx 1.9\times10^{-4}\,\mathrm{Gyr}^{-1}$. The Hubble parameter is employed as universal scaling variable, determining the redshift evolution of the gravitational constant as well as of SN Ia and AGN luminosities. The motivation is Dirac's hypothesis that moderate dimensionless ratios composed of the fundamental constants stay constant in the cosmic evolution, whereas large ratios vary with time, having been small in the past (Dirac 1938; Dyson 1972).

We start with a Hubble diagram of Type Ia supernovae extending to redshifts $z \approx 1.75$ (Riess et al. 2007; Wood-Vasey et al. 2007). The scaling exponent of the luminosity $L \propto H^{-\lambda}(z)$ is treated as a fitting parameter, and we find a linear dependence of the SN Ia luminosity on the Hubble parameter, reminiscent of the metallicity correction to SN Ia magnitudes suggested in Gallagher et al. (2008). We then turn to the redshift scaling of the AGN luminosity function, and perform a fit to the comoving AGN/QSO

space density (Hasinger et al. 2005; Silverman et al. 2005; Richards et al. 2006). Finally, we perform a fit to several ROSAT, XMM-Newton, and Chandra number counts of soft X-ray point sources (Brunner et al. 2008; Carrera et al. 2007; Cappelluti et al. 2009; Elvis et al. 2009), which provides a test of the scaling exponents of the luminosity function used in the fit of the AGN space density.

In Sect. 2, we briefly sketch the general formalism, starting with a Robertson–Walker line element and a negatively curved open 3-space. We discuss the parametrization of the cosmic expansion factor in terms of asymptotic exponents defining the early and late stage of the expansion, as well as the corresponding Hubble parameter, the luminosity distance, and the flux-redshift relation. The redshift scaling $G \propto H(z)$ of the gravitational constant is inferred from the constant ratio $4\pi\hbar^2 H_0/(G_0 c m_\pi^3) \approx 1$. The second moderate dimensionless ratio considered is $G_0 L_{\mathrm{G},0}/\upsilon_{\mathrm{G},0}^5$, where $L_{\mathrm{G},0}$ denotes the Galactic luminosity and $\upsilon_{\mathrm{G},0}$ the velocity of the Galaxy in the microwave background. (Zero subscripts indicate present-day values.) The constancy of this ratio suggests a redshift evolution of galactic luminosities affecting the AGN space density (see Sect. 5) as well as the number counts of X-ray point sources studied in Sect. 6.

In Sect. 3, we perform the redshift parametrization of the comoving distance, luminosity distance, and Hubble parameter, and calculate their high-z asymptotics. In Sect. 4, we derive the low-z expansions of these quantities, as well as their ascending series in look-back time, and we plot the Hubble diagram for a compilation of SN Ia distance moduli, from which the Type Ia luminosity scaling $\propto H(z)$ is inferred.

The comoving space density of active galactic nuclei (AGNs) and quasars (QSOs) is studied in Sect. 5. The redshift evolution of the AGN luminosity function is related to a third moderate ratio, $G_0\rho_{\mathrm{m}}/H_0^2$, involving the present-day mass density ρ_{m} of the universe. We show that the AGN space density, in particular, its initial steep increase, can be fitted with scaling exponents ensuring the constancy of this ratio.

Flux-limited number counts of X-ray point sources are investigated in Sect. 6. The differential and cumulative counts are derived from the luminosity function studied in Sect. 5. We discuss the high-flux and low-flux asymptotics of the counting functions, and derive a numerically efficient integral representation of the crossover. The cumulative counting function is fitted to a compilation of source counts in the soft X-ray band, with scaling exponents extracted from the AGN space density. In Sect. 7, we summarize our conclusions.

2 Gravitational constant and Hubble parameter: scaling relations derived from the constancy of moderate dimensionless ratios

We consider an open Robertson–Walker cosmology with line element (Sandage 1988)

$$\begin{aligned} \mathrm{d}s^2 &= -c^2\,\mathrm{d}\tau^2 + a^2(\tau)\,\mathrm{d}\sigma^2, \\ \mathrm{d}\sigma^2 &= 4\bigl(1-|\mathbf{x}|^2/R^2\bigr)^{-2}\,\mathrm{d}\mathbf{x}^2, \end{aligned} \tag{2.1}$$

where $\mathrm{d}\sigma^2$ is the metric of the ball model of hyperbolic geometry, $|\mathbf{x}| < R$. The curvature radius of the negatively curved open 3-space is $a(\tau)R$. Without loss of generality, we set $a(\tau_0) = 1$, so that the sectional 3-space curvature at the present epoch τ_0 is $-1/R^2$. The following discussion remains valid for a Euclidean 3-space geometry, $R \to \infty$. The factor of 4 in (2.1) is customary in hyperbolic geometry, resulting in a sectional curvature of $-1/(a(\tau)R)^2$, and can be removed by a rescaling of the length unit. Recent Wilkinson Microwave Anisotropy Probe (WMAP) and Sloan Digital Sky Survey (SDSS) estimates of the baryon and total matter densities have revived the interest in testing negatively curved 3-space geometries (Komatsu et al. 2009; Reid et al. 2009; Percival et al. 2009; Kessler et al. 2009).

The ascending series of the dimensionless scale factor $a(\tau)$ reads

$$a(\tau) = 1 + \Delta - (q_0/2)\Delta^2 + (p_0/6)\Delta^3 + \cdots, \tag{2.2}$$

where we use the shortcut $\Delta := H_0 \cdot (\tau - \tau_0)$. Subscript zeros refer to the present epoch τ_0, so that $H_0 = H(\tau_0)$, where $H(\tau) = \dot{a}(\tau)/a(\tau)$ is the Hubble parameter. The second order in (2.2) is determined by the (deceleration) parameter $q_0 = -\ddot{a}_0/\dot{a}_0^2$, and the third by $p_0 = a_0^{(3)}/\dot{a}_0^3$. Present epoch (absorption time) and emission time are denoted by τ_0 and τ_1, respectively, so that $\tau_0 > \tau_1$. We will use the rescaled dimensionless look-back interval $\Delta_1 = H_0 \cdot (\tau_1 - \tau_0)$; the look-back time is $\tau_0 - \tau_1$, so that Δ_1 is negative.

The present-day gravitational constant is $G_0 \approx 6.707 \times 10^{-45}\hbar c^5\ \mathrm{MeV}^{-2}$ (Amsler et al. 2008). The constancy of the moderate ratio (Tomaschitz 2000)

$$\frac{\hbar^2 H_0}{G_0 c m_\pi^3} \approx \frac{1}{4\pi} \tag{2.3}$$

requires the variation of the gravitational constant to be proportional to the Hubble parameter,

$$\frac{G(\tau)}{G_0} = \frac{H(\tau)}{H_0}. \tag{2.4}$$

The pion mass, $m_\pi \approx 139.567\ \mathrm{MeV}/c^2$, is constant in the cosmic evolution, and so is Planck's constant and the speed of light. Particle masses, the fine structure constant, and the subatomic interaction constants are kept constant, in contrast to Dirac's large numbers hypothesis (Dirac 1938). There are

stringent bounds on the variation of these constants, coming from various quarters of physics, which make a time variation within the age of the Earth unlikely (Tomaschitz 1998, 2000). The numerical relation (2.3) is satisfied by choosing $H_0 = h_0/(9.7781\ \text{Gyr})$ with $h_0 \approx 0.6802$, so that $H_0^{-1} \approx 14.375$ Gyr. Some observational estimates of h_0 are quite close to this value (Ferrarese et al. 2000; Jimenez et al. 2003; Sandage et al. 2006; Reid et al. 2009; Percival et al. 2009). Conversions are based on $c/H_0 \approx 2.9979 \times 10^3/h_0$ Mpc and 1 Gyr $\approx 3.1557 \times 10^{16}$ s.

An excellent estimate of the deceleration parameter q_0 is obtained from bounds on the present-day logarithmic derivative of G, such as $|\dot{G}_0/G_0| < 1.6 \times 10^{-3}$ Gyr^{-1} inferred from helioseismology (Guenther et al. 1998). The tightest bounds are obtained from lunar laser ranging, $(4 \pm 9) \times 10^{-4}$ Gyr^{-1} (Williams et al. 2006) and $(2 \pm 7) \times 10^{-4}$ Gyr^{-1} (Müller and Biskupek 2007). These bounds suggests a q_0 very close to -1 by virtue of, see (2.4),

$$\dot{G}_0/G_0 = -H_0\varepsilon, \quad \varepsilon := 1 + q_0. \tag{2.5}$$

The bound of 2×10^{-4} Gyr^{-1} implies $|\varepsilon| < 2.9 \times 10^{-3}$.

We study a specific class of expansion factors (Tomaschitz 2005),

$$a(\tau) = A_0 \tau^\beta \sinh^\alpha(\eta\tau/\tau_0), \tag{2.6}$$

describing the crossover from an initial power law, $\propto \tau^{\alpha+\beta}$, to exponential expansion, $\propto \tau^\beta e^{\alpha\eta\tau}$, in the final stage. The parameters α and η are positive, and $\gamma := \alpha + \beta \geq 0$. The latter condition is required for expansion, that is, $\dot{a}(\tau) > 0$ throughout the evolution. The normalization $A_0 := 1/(\tau_0^\beta \sinh^\alpha \eta)$ gives $a(\tau_0) = 1$. The logarithmic derivative of (2.6) is

$$H(\tau) = \frac{\alpha\eta}{\tau_0} \coth\left(\eta\frac{\tau}{\tau_0}\right) + \frac{\beta}{\tau}. \tag{2.7}$$

If $\gamma > 0$, we find $H(\tau \to 0) \sim \gamma/\tau$ and $H(\tau \to \infty) \sim \alpha\eta/\tau_0$. As mentioned, $\gamma = \alpha + \beta$, and we define $n := 1/\gamma$ for future reference.

The parameters τ_0, q_0, and p_0 in the ascending series (2.2) are related to the expansion factor (2.6) as

$$H_0\tau_0 = \alpha\eta \coth\eta + \beta, \tag{2.8}$$

$$\varepsilon := q_0 + 1 = \frac{1}{(H_0\tau_0)^2}\left(\frac{\alpha\eta^2}{\sinh^2\eta} + \beta\right), \tag{2.9}$$

$$\delta := p_0 - 1 = \frac{2}{(H_0\tau_0)^3}\left(\alpha\eta^3\frac{\coth\eta}{\sinh^2\eta} + \beta\right) - 3\varepsilon. \tag{2.10}$$

Paleoclimatic estimates of planetary surface temperatures were used in Tomaschitz (2005) to single out the expansion factor defined by

$$\alpha = 1, \qquad \beta = -1/2, \qquad \eta = 3/2, \tag{2.11}$$

so that $H_0\tau_0 \approx 1.1572$, see (2.8). This results in a cosmic age of $\tau_0 \approx 16.635$ Gyr and a deceleration parameter defined by $\varepsilon \approx -2.786 \times 10^{-3}$, see (2.9), which determines the present-day logarithmic derivative, $\dot{G}_0/G_0 \approx 1.938 \times 10^{-4}$ Gyr^{-1}, according to (2.5). For comparison, the averaged Th/Eu age of three M15 giants is estimated as 14 ± 3 Gyr (Sneden et al. 2000), and the age of the halo star CS 31082–001 is 15.5 ± 3.2 Gyr inferred from U/Th production ratios (Schatz et al. 2002; Cowan and Sneden 2006). A combined estimate based on U/Th abundance ratios in meteorites and halo stars gives a Galactic age of $14.5^{+2.8}_{-2.2}$ Gyr (Dauphas 2005).

The derivative of the Hubble parameter (2.7) reads

$$\dot{H}(\tau) = -\frac{\alpha\eta^2}{\tau_0^2}\frac{1}{\sinh^2(\eta\tau/\tau_0)} - \frac{\beta}{\tau^2}, \tag{2.12}$$

so that $\dot{H}(\tau \to 0) \sim -\gamma/\tau^2$ and $\dot{H}(\tau \to \infty) \sim -\beta/\tau^2$. The comoving distance between emission at τ_1 and absorption at τ_0 is (Sandage 1988, 1995)

$$D(\tau_0, \tau_1) := c\int_{\tau_1}^{\tau_0} \frac{\mathrm{d}\tau}{a(\tau)}. \tag{2.13}$$

This is the metric distance at absorption time τ_0, according to the line element $\mathrm{d}\sigma^2$ in (2.1); the distance at emission time is $a(\tau_1)D(\tau_0, \tau_1)$. $D(\tau_0, \tau_1)$ is regarded as a function of τ_0 and redshift (rather than τ_1), by inversion of

$$a(\tau_1) = 1/(1+z), \tag{2.14}$$

and $a(\tau_0) = 1$ is assumed here. We write $D(z)$ as a shortcut for $D(\tau_0, \tau_1(z))$, suppressing the argument τ_0. Differentiating (2.13) and (2.14), we find the identities

$$\frac{\mathrm{d}z}{\mathrm{d}\tau_1} = -\frac{H(\tau_1)}{a(\tau_1)}, \quad H(\tau_1)\tau_1'(z) = -\frac{1}{1+z}. \tag{2.15}$$

As for the comoving distance,

$$\frac{\mathrm{d}D}{\mathrm{d}\tau_1} = -\frac{c}{a(\tau_1)}, \quad D'(z) = \frac{c}{H(\tau_1)}, \quad D(z) = c\int_0^z \frac{\mathrm{d}z}{H(z)}. \tag{2.16}$$

Writing $H(z)$ as a shortcut for $H(\tau_1(z))$, we obtain, see (2.7), (2.12), and (2.15),

$$H'(z) = -\frac{1}{1+z}\frac{\dot{H}(\tau_1)}{H(\tau_1)}, \tag{2.17}$$

which allows us to calculate the redshift derivative of the Hubble parameter without invoking the derivative of $\tau_1(z)$. This is convenient, since $\tau_1(z)$ is found by numerical inversion of the expansion factor, see (3.1).

We introduce the normalized Hubble parameter $h(z) := H(z)/H_0$, and write the curvature radius as $R =: \hat{R}c/H_0$,

so that $\hat{R}$ is just the present-day curvature radius in units of c/H_0. Hence, see (2.16),

$$\frac{D'(z)}{R} = \frac{1}{\hat{R}h(z)}, \quad \frac{D(z)}{R} = \frac{1}{\hat{R}}\int_0^z \frac{\mathrm{d}z}{h(z)}. \tag{2.18}$$

The area of a sphere of radius D in hyperbolic space is

$$\mathrm{area}(D) = 4\pi R^2 \sinh^2(D/R), \tag{2.19}$$

and the enclosed volume reads

$$V(D) = \int_0^D \mathrm{area}(D)\,\mathrm{d}D = \pi R^3\left(\sinh\frac{2D}{R} - \frac{2D}{R}\right). \tag{2.20}$$

The curvature radius R and the comoving distance $D(z)$ as well as the comoving volume $V(D(z))$ are present-day values at τ_0. At emission time τ_1, the line element of the 3-space is $a^2(\tau_1)\,\mathrm{d}\sigma^2$, and the curvature radius is $a(\tau_1)R$, see (2.1). The area of a hyperbolic sphere scales as $a^2(\tau_1)\mathrm{area}(D)$, and the volume of a redshift shell $\mathrm{d}z$ as $a^3(\tau_1(z))\,\mathrm{d}V(D(z))$, where $\mathrm{d}V(D) = \mathrm{area}(D)\,\mathrm{d}D$.

The intrinsic luminosity L_b of a source is related to the apparent flux S_b by the flux-redshift relation

$$S_\mathrm{b} = \frac{L_\mathrm{b}}{4\pi d_\mathrm{L}^2}, \quad d_\mathrm{L}(z) := (1+z)R\sinh\frac{D(z)}{R}, \tag{2.21}$$

where d_L is the luminosity distance, see (2.19). We here assume frequency-integrated bolometric quantities. The factor $(1+z)^{-2}$ stems from the energy shift $\nu_1/\nu_0 = 1+z$ and the time dilation $\mathrm{d}t_1/\mathrm{d}t_0 = 1/(1+z)$. In the Euclidean limit, $\sinh(D/R)$ is replaced by D/R.

We may consider spectral densities instead of bolometric quantities, $S_\mathrm{b} = \int_0^\infty S(\nu)\,\mathrm{d}\nu$, $L_\mathrm{b} = \int_0^\infty L(\nu)\,\mathrm{d}\nu$, so that

$$S(\nu_0) = \frac{L(\nu_1)(1+z)}{4\pi d_\mathrm{L}^2(z)}, \tag{2.22}$$

which can be written as (Sandage 1988)

$$S(\nu_0) = \frac{L(\nu_0)K(z)}{4\pi d_\mathrm{L}^2(z)}, \qquad K(z) := \frac{L((1+z)\nu_0)}{L(\nu_0)}(1+z). \tag{2.23}$$

In the case of a power-law density, $L \propto \nu^{-s}$, we find $K = (1+z)^{1-s}$. The X-ray photon index $\Gamma = s+1$ has a typical range of $1.4 \le \Gamma \le 2.4$. We thus find the spectral flux-redshift relation

$$S = \frac{L}{4\pi}\frac{(1+z)^{1-s}}{d_\mathrm{L}^2(z)}, \tag{2.24}$$

where S and L are spectral densities (per unit frequency). At $s = 1$, this coincides with the bolometric relation (2.21).

Finally, we consider a galactic luminosity evolution $L(z) = L_0 h^{-\lambda}(z)$, where L is the intrinsic luminosity at emission time $\tau_1(z)$, and L_0 is the present-day luminosity at τ_0. To relate this scaling to a moderate ratio, we start with $G_0/c^5 \approx 2.756\times10^{-60}$ s/erg, and note that $\upsilon_{\mathrm{G},0}/c \approx 1/478$ and $L_{\mathrm{G},0} \approx 2\times10^{10}L_\odot \approx 7.7\times10^{43}$ erg/s, where $\upsilon_{\mathrm{G},0}$ is the velocity of the Galaxy in the microwave background and $L_{\mathrm{G},0}$ its luminosity (Amsler et al. 2008). We thus find

$$\frac{G_0 L_{\mathrm{G},0}}{\upsilon_{\mathrm{G},0}^5} \approx \frac{1}{190}. \tag{2.25}$$

On substituting $L_\mathrm{G} = L_{\mathrm{G},0}h^{-\lambda}(z)$, $\upsilon_\mathrm{G} = \upsilon_{\mathrm{G},0}h^{-\vartheta}(z)$, and $G = G_0 h(z)$ into $GL_\mathrm{G}/\upsilon_\mathrm{G}^5$, we obtain $\lambda = 5\vartheta + 1$ as a condition on the exponents for this ratio to stay constant.

3 High-redshift asymptotics of comoving distance and Hubble parameter

To put the redshift scaling discussed in Sect. 2 to test, we need to make it more explicit by specifying the space expansion. We study expansion factors of type (2.6), defined by parameters α, β, and η, which determine the asymptotic stages $\tau \to 0, \infty$. The expansion factor defined by the parameter set (2.11) is used in the fits in Figs. 1, 2 and 3, but otherwise we do not specify these parameters in the high- and low-z expansions in Sects. 3 and 4.

The emission time is parametrized by redshift, by solving $a(\tau_1) = 1/(1+z)$ or

$$\big(\eta\tau_1(z)/\tau_0\big)^{\beta/\alpha}\sinh\big(\eta\tau_1(z)/\tau_0\big) = \frac{\eta^{\beta/\alpha}\sinh\eta}{(1+z)^{1/\alpha}}. \tag{3.1}$$

In all high-z expansions ($\tau_1 \to 0$), we use $1+z$ or some power thereof as expansion parameter. The two leading orders of the asymptotic inversion of (3.1) read

$$\frac{\tau_1(z)}{\tau_0} = \frac{x}{\eta}\left(1 - \frac{1}{6}\frac{\alpha}{\gamma}x^2 + \mathrm{O}\big(x^4\big)\right), \qquad x(z) := \frac{\eta^{\beta n}\sinh^{\alpha n}\eta}{(1+z)^n}, \tag{3.2}$$

where $\gamma = \alpha+\beta > 0$, and $n = 1/\gamma$. Upon specializing these parameters as in (2.11), we find

$$\frac{\tau_1(z)}{\tau_0} = \frac{2.015}{(1+z)^2}\left(1 - \frac{3.045}{(1+z)^4} + \cdots\right). \tag{3.3}$$

We turn to the high-z expansion of the metric distance $D(z)$, see (2.13),

$$D(z) := D(\tau_0,\tau_1) = c\tau_0\sinh^\alpha(\eta)\int_{\tau_1/\tau_0}^1 \frac{\mathrm{d}t}{t^\beta\sinh^\alpha(\eta t)}. \tag{3.4}$$

The z dependence is via $\tau_1(z)$ in the lower integration boundary, by inversion of (3.1). From now on, we restrict the parameter range to $0 < \alpha+\beta < 1$, so that the integral stays

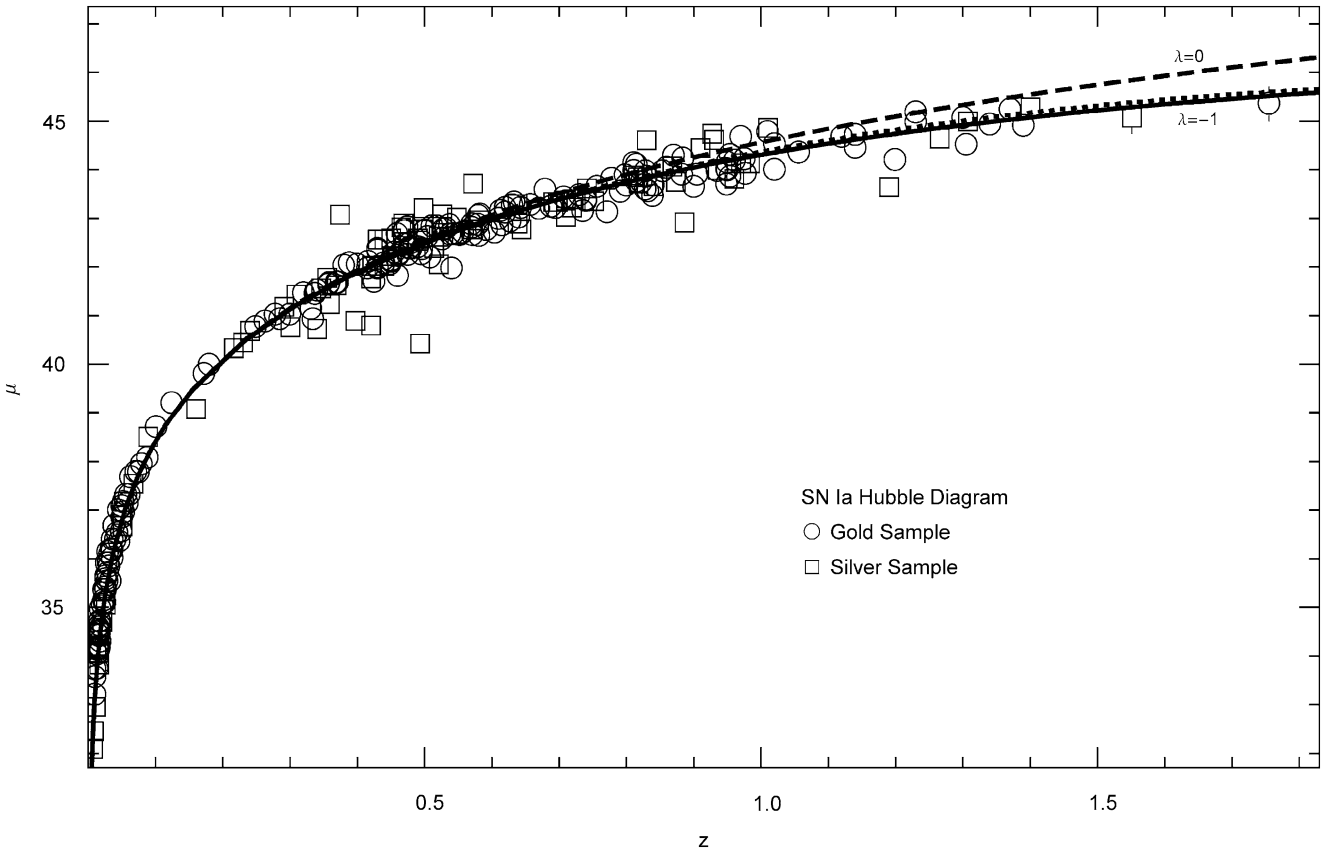

Fig. 1 SN Ia Hubble diagram. Data points compiled from a listing of ground-discovered SNe Ia, comprising ESSENCE and SNLS samples as well as a sample of nearby SNe Ia (Wood-Vasey et al. 2007), and from Riess et al. (2007) recording HST-discovered SNe Ia. The fit is performed with the distance modulus $\mu = 5\log(h^{\lambda/2}d_{\mathrm{L}}/\mathrm{Mpc}) + 25$, see text after (4.10), where $d_{\mathrm{L}}(z)$ denotes the luminosity distance (2.21), $h(z)$ the normalized Hubble parameter, see (2.18), and λ the scaling exponent of the SN Ia luminosity, $L \propto h^{-\lambda}(z)$. The *solid curve* depicts the fit at $\lambda = -1$, and the *dotted one* the low-z expansion of $\mu(z, \lambda = -1)$, see (4.10) and (4.15), applicable to redshifts up to about $z \approx 2.2$, where it falls off. The high-z asymptote is the upper edge of the figure at $\mu(\infty, \lambda = -1) \approx 47.36$. The *dashed curve* shows the modulus $\mu(z, \lambda = 0)$ in the absence of luminosity evolution. The criteria for the Gold and Silver data sets are defined in Riess et al. (2007); the fit can be compared to Fig. 6 of this reference

finite for $\tau_1 \to 0$, as suggested by planetary paleoclimates (Tomaschitz 2005). Expanding $D(z)$ in ascending powers of τ_1/τ_0, we obtain

$$D(z) = c\tau_0 \sinh^{\alpha}(\eta)\biggl(\sigma_{\mathrm{h}} - \frac{\eta^{\beta-1}}{1-\gamma}(\eta\tau_1/\tau_0)^{1-\gamma} \times \biggl(1 - \frac{\alpha}{6}\frac{1-\gamma}{3-\gamma}(\eta\tau_1/\tau_0)^2 + \cdots\biggr)\biggr), \tag{3.5}$$

where we have introduced the shortcut

$$\sigma_{\mathrm{h}} := \int_0^1 \frac{\mathrm{d}s}{s^{\beta}\sinh^{\alpha}(\eta s)}. \tag{3.6}$$

The ellipsis stands for terms of $\mathrm{O}((\tau_1/\tau_0)^4)$, and $\gamma = \alpha + \beta$, so that $n = 1/\gamma > 1$, see the text after (2.7). In (3.5), we substitute the high-z expansion (3.2) of τ_1/τ_0,

$$\frac{D(z)}{R} = D_{\infty} - D_{\mathrm{h}}(z), \quad D_{\infty} := \frac{H_0\tau_0}{\hat{R}}\sigma_{\mathrm{h}}\sinh^{\alpha}\eta, \tag{3.7}$$

$$D_{\mathrm{h}}(z) := \frac{H_0\tau_0}{\hat{R}}\frac{\eta^{\beta-1}\sinh^{\alpha}\eta}{1-\gamma}x^{1-\gamma} \times \biggl(1 - \frac{\alpha}{2\gamma}\frac{1-\gamma}{3-\gamma}x^2 + \mathrm{O}\bigl(x^4\bigr)\biggr), \tag{3.8}$$

with $x(z)$ as defined in (3.2) and σ_{h} in (3.6). $\hat{R}$ is the present-day curvature radius of the hyperbolic 3-space in units of c/H_0, so that $R = \hat{R}c/H_0$ and $c\tau_0/R = H_0\tau_0/\hat{R}$. The metric distance of the horizon is RD_{∞}, and the correction $RD_{\mathrm{h}}(z)$ accounts for finite z. More explicitly,

$$D_{\mathrm{h}}(z) = \frac{d_{\infty}}{(1+z)^{n-1}}\biggl(1 + \frac{d_1}{(1+z)^{2n}} + \mathrm{O}\bigl((1+z)^{-4n}\bigr)\biggr),$$
$$d_{\infty} := \frac{H_0\tau_0}{\hat{R}}\frac{\eta^{\beta n}\sinh^{\alpha n}\eta}{(1-\gamma)\eta},$$
$$d_1 := -\frac{\alpha}{2\gamma}\frac{1-\gamma}{3-\gamma}\eta^{2\beta n}\sinh^{2\alpha n}\eta. \tag{3.9}$$

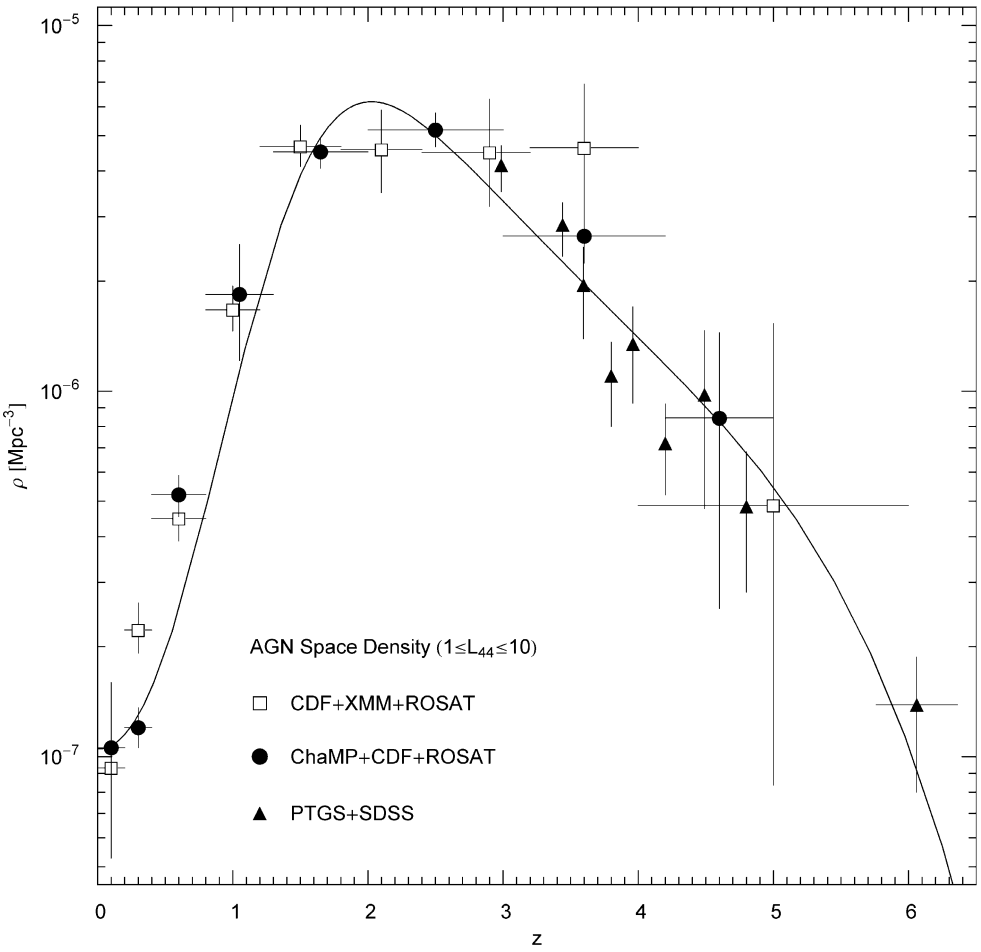

Fig. 2 AGN space density. CDF + XMM + ROSAT data points from Hasinger et al. (2005), ChaMP + CDF + ROSAT points from Silverman et al. (2005). PTGS + SDSS triangles stand for optically selected QSOs, scaled to match the X-ray data (Fan et al. 2001, 2004; Richards et al. 2006; Schmidt et al. 1995); also see Wall et al. (2005) and Wolf et al. (2003). The fit is performed with the comoving space density (5.15) composed of two competing power laws, the first generating the initial steep increase, the second a more moderate decline terminating in exponential decay (5.18). The input and fitting parameters are given after (5.16)

The high-z asymptotics of the comoving volume (2.20) and the luminosity distance (2.21) is found by splitting the comoving distance $D(z)$ as in (3.7) and substituting expansion (3.9) into $\sinh(D_\infty - D_\mathrm{h})$. (It is not efficient to further expand the hyperbolic sine in ascending powers of D_h because of slow convergence.)

The fits in Figs. 1–3 are performed with the input parameters (2.11),

$$\alpha = 1, \qquad \beta = -\frac{1}{2}, \qquad \eta = \frac{3}{2},$$
$$\gamma = \alpha + \beta = \frac{1}{2}, \qquad n = \frac{1}{\gamma} = 2, \tag{3.10}$$

which give, see (2.8) and the text after (2.11),

$$H_0\tau_0 \approx 1.157, \quad \tau_0 \approx 11.315/h_0 \text{ Gyr}, \tag{3.11}$$

as well as $\sigma_\mathrm{h} \approx 1.246$ for integral (3.6). We also note that $c/H_0 \approx 2.998 \times 10^3/h_0$ Mpc, where $h_0 \approx 0.680$, see the text after (2.4). The numerical constants in (3.7) and (3.9) are

$$D_\infty \approx 3.070/\hat{R}, \qquad d_\infty \approx 4.664/\hat{R},$$
$$d_1 \approx -1.827. \tag{3.12}$$

A horizon emerges as a hyperbolic sphere of radius $D(z = \infty)$, that is, $D(\tau_0, 0) = RD_\infty \approx 9.203 \times 10^3/h_0$ Mpc; only photons emitted within this sphere can be received at the present epoch. There is also an event horizon, defined by the metric distance $D(\infty, \tau_0)$, see (3.4); photons emitted at the present epoch outside this sphere cannot reach us in the future. The radius of this horizon is calculated as $D(\infty, \tau_0) = RD_\infty(\sigma_\mathrm{h} \to \sigma_\mathrm{e})$, see (3.7), with σ_h replaced by $\sigma_\mathrm{e} := \int_1^\infty s^{-\beta} \sinh^{-\alpha}(\eta s)\,\mathrm{d}s$. Hence, $D(\infty, \tau_0) = (\sigma_\mathrm{e}/\sigma_\mathrm{h})D(\tau_0, 0)$. The expansion specified in (3.10) gives $\sigma_\mathrm{e} \approx 0.3834$, so that $D(\infty, \tau_0) \approx 0.308D(\tau_0, 0)$.

The ascending τ/τ_0 series of the Hubble parameter (2.7) reads

$$\frac{H^\lambda(\tau)}{H_0^\lambda} = \frac{(\eta\gamma)^\lambda}{(H_0\tau_0)^\lambda}\frac{1}{y^\lambda}\left(1 + \frac{\alpha\lambda}{3\gamma}y^2 + \frac{\alpha\lambda}{9\gamma}\left(\frac{\alpha}{\gamma}\frac{\lambda - 1}{2} - \frac{1}{5}\right)y^4 + \mathrm{O}\big(y^6\big)\right), \tag{3.13}$$

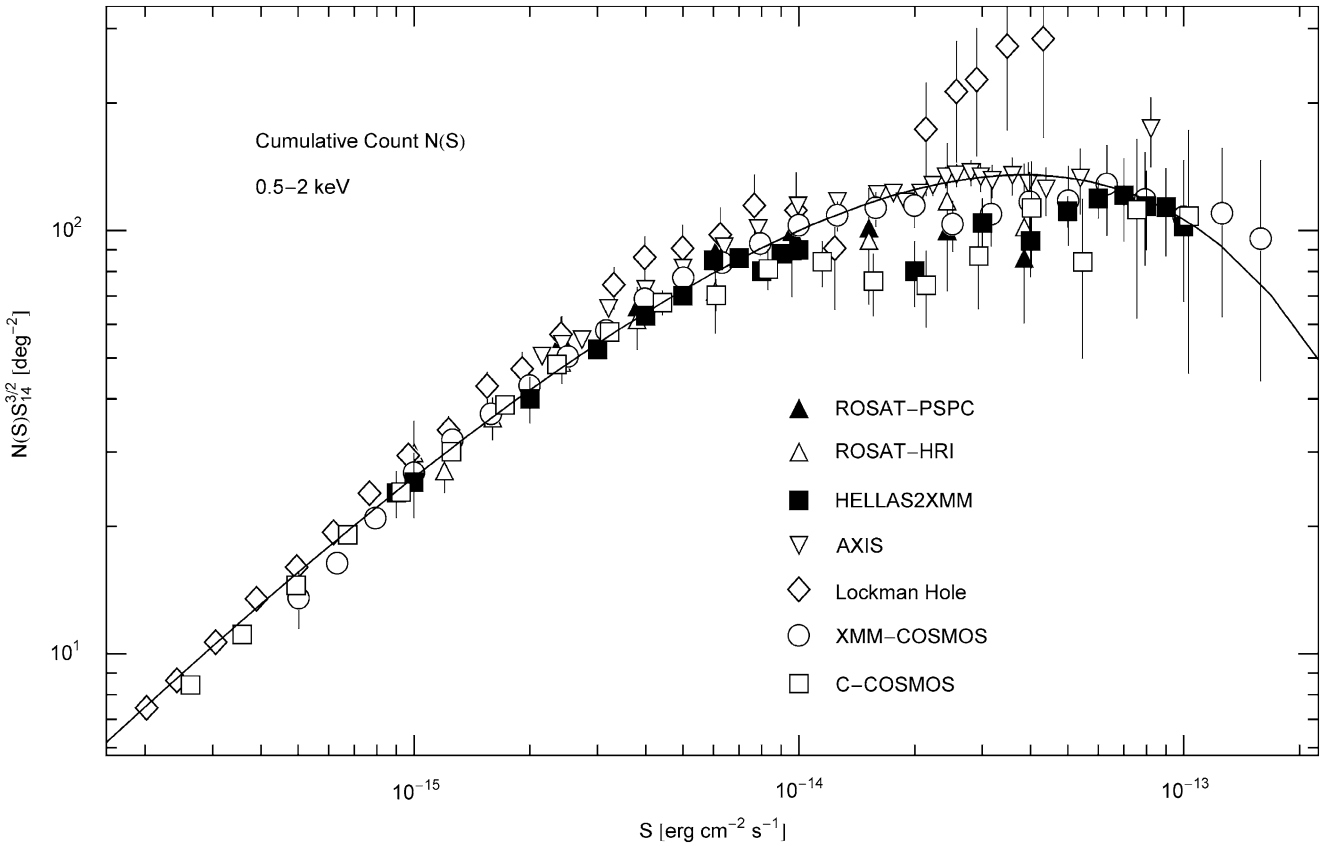

Fig. 3 Cumulative number count of soft X-ray point sources (0.5–2 keV). ROSAT-PSPC and HRI data points from Hasinger et al. (1998), HELLAS2XMM sources from Baldi et al. (2002), Lockman Hole sources from Brunner et al. (2008), AXIS points from Carrera et al. (2007), XMM-COSMOS wide-field data from Cappelluti et al. (2009), and Chandra-COSMOS points from Elvis et al. (2009); also see Bauer et al. (2004), Gilli et al. (2007), Lehmer et al. (2005), Moretti et al. (2003), Puccetti et al. (2006), Rosati et al. (2002), and Ueda et al. (2008). The count $N(S)$ is rescaled by a factor $S_{14}^{3/2}$, which refers to the Euclidean high-S scaling (6.33), so that the latter corresponds to a *horizontal straight line* in this double-logarithmic plot, with ordinate at about 2.3×10^3. This Euclidean regime is not attained because of the exponential cutoff (6.18). (There are indications that the deviation from the Euclidean high-flux scaling is even more pronounced in the hard X-ray bands; see the above references, the data sets are sparser though.) The fit is based on the integral representation (6.28) of $N(S)$, with parameters listed at the end of Sect. 6

where $y := \eta\tau/\tau_0$ and λ is an arbitrary real power. The high-z asymptotics is found by substituting expansion (3.2) of $\tau_1(z)$ for τ. As in (2.18), we use the rescaled parameter $h(z) = H(\tau_1(z))/H_0$ to obtain

$$h(z) = h_\infty(1+z)^n\biggl(1+\frac{h_1}{(1+z)^{2n}} + \mathrm{O}\bigl((1+z)^{-4n}\bigr)\biggr), \tag{3.14}$$

$$h_\infty := \frac{\gamma\eta}{H_0\tau_0}\frac{1}{(\eta^\beta\sinh^\alpha\eta)^n}, \qquad h_1 := \frac{\alpha}{2\gamma}\bigl(\eta^\beta\sinh^\alpha\eta\bigr)^{2n}. \tag{3.15}$$

The constants in (3.10) and (3.11) give

$$n = 2, \qquad h_\infty \approx 0.2144, \qquad h_1 \approx 9.136. \tag{3.16}$$

The high-z expansion of the redshift derivative of the comoving volume, see (5.5) and (5.19), can readily be assembled from (3.7), (3.9), and (3.14).

4 SN Ia Hubble diagram

4.1 Emission time and comoving distance in the low-redshift regime

The low-z parametrization of the emission time reads

$$\frac{\tau_1(z)}{\tau_0} - 1 = \frac{\Delta_1}{H_0\tau_0} = -\frac{z}{H_0\tau_0}\biggl(1-\frac{1}{2}(1+\varepsilon)z + \biggl(\frac{1}{3}-\frac{\delta}{6}+\frac{\varepsilon^2}{2}\biggr)z^2+\cdots\biggr), \tag{4.1}$$

where $\Delta_1 = H_0 \cdot (\tau_1 - \tau_0)$. Here, we used the ascending series (2.2) of the expansion factor to invert $a(\tau_1(z)) = 1/(1+z)$, with $\varepsilon = q_0 + 1$, $\delta = p_0 - 1$ (see (2.9) and (2.10)), and the convention $a(\tau_0) = 1$. Specifying the expansion factor as in (3.10), we find

$$\varepsilon \approx -2.786 \times 10^{-3}, \qquad \delta \approx 0.4245, \tag{4.2}$$

and the low-z expansion of $\tau_1(z)$,

$$\tau_1(z)/\tau_0 = 1 - 0.864z\big(1 - 0.499z + 0.263z^2 + \cdots\big), \tag{4.3}$$

normalized with the present epoch τ_0, see (3.11). We also note the ascending z series of an arbitrary real power λ of the look-back interval $-\Delta_1$,

$$(-\Delta_1)^\lambda = z^\lambda\bigg(1 - \frac{\lambda}{2}(1+\varepsilon)z + \lambda\bigg(\frac{5+3\lambda-4\delta}{24} + \frac{\lambda-1}{4}\varepsilon + \frac{\lambda+3}{8}\varepsilon^2\bigg)z^2 + \cdots\bigg). \tag{4.4}$$

The low-z expansion of the comoving distance $D(z)$ is likewise based on the ascending series (2.2) of the expansion factor,

$$\frac{1}{a(\tau)} = 1 - \Delta + \bigg(1 + \frac{q_0}{2}\bigg)\Delta^2 - \bigg(1 + q_0 + \frac{p_0}{6}\bigg)\Delta^3 + \cdots, \tag{4.5}$$

and subsequent term-by-term integration in (2.13). The ascending series in look-back time of an arbitrary power of $D(\tau_0, \tau_1)$ reads

$$D^\lambda(\tau_0,\tau_1) = \bigg(-\frac{c}{H_0}\Delta_1\bigg)^\lambda\bigg(1 - \frac{\lambda}{2}\Delta_1 + \frac{\lambda}{24}(1 + 3\lambda + 4\varepsilon)\Delta_1^2 + \cdots\bigg). \tag{4.6}$$

Here, we substitute expansion (4.4) of the look-back interval to find

$$D^\lambda(z) = \bigg(\frac{c}{H_0}z\bigg)^\lambda\bigg(1 - \frac{1}{2}\varepsilon\lambda z - \lambda\bigg(\frac{\delta}{6} + \frac{\varepsilon}{3} - \frac{\lambda+3}{8}\varepsilon^2\bigg)z^2 + \cdots\bigg), \tag{4.7}$$

where λ is a real power, and the parameters ε and δ are related to expansion factor (2.6) as stated in (2.9) and (2.10).

4.2 Luminosity distance and distance modulus: SN Ia luminosity evolution

The low-z expansion of the luminosity distance (2.21) is

$$d_\mathrm{L}(z) = \frac{c}{H_0}z(1+z)\bigg(1 - \frac{1}{2}\varepsilon z + \bigg(\frac{1}{6\hat{R}^2} - \frac{\delta}{6} - \frac{\varepsilon}{3} + \frac{1}{2}\varepsilon^2\bigg)z^2 + \mathrm{O}\big(z^3\big)\bigg), \tag{4.8}$$

with coefficients ε and δ defined in (2.9), (2.10), and (4.2). To derive this, we have used in (2.21) the ascending $D(z)$ series of the hyperbolic sine with the low-z expansion (4.7) substituted:

$$\sinh^\lambda\frac{D(z)}{R} = \frac{z^\lambda}{\hat{R}^\lambda}\bigg(1 - \frac{\lambda}{2}\varepsilon z + a_2 z^2 + \cdots\bigg), \qquad a_2(\lambda) := \lambda\bigg(\frac{1}{6\hat{R}^2} - \frac{\delta}{6} - \frac{\varepsilon}{3} + \frac{\lambda+3}{8}\varepsilon^2\bigg), \tag{4.9}$$

where λ is an arbitrary real power. The constants (4.2) give

$$d_\mathrm{L}(z) = \frac{c}{H_0}z(1+z)\bigg(1 + 1.39 \times 10^{-3}z + \bigg(\frac{1}{6\hat{R}^2} - 6.98 \times 10^{-2}\bigg)z^2 + \cdots\bigg). \tag{4.10}$$

The dependence of the luminosity distance on the curvature radius $\hat{R}$ (in units of c/H_0, see (2.18)) only shows in the second-order correction.

We consider an intrinsic luminosity evolution $L_\mathrm{b} \propto h^{-\lambda}(z)$ in the bolometric flux-redshift relation (2.21), so that $S(z) \propto 1/(h^\lambda d_\mathrm{L}^2)$. The distance modulus is then defined as $\mu = 5\log(h^{\lambda/2}(z)d_\mathrm{L}(z)[\mathrm{Mpc}]) + 25$ (Riess et al. 2004; Sandage 1988). Figure 1 depicts the SN Ia Hubble diagram covering redshifts up to $z \approx 1.75$ (Riess et al. 2007; Wood-Vasey et al. 2007). μ is compiled with the Hubble parameter (2.7), the luminosity distance in (2.21), and the integral representation (3.4) of the comoving distance; the redshift parametrization is obtained by inversion of (3.1). The fit is performed with a linear luminosity evolution, $\lambda = -1$, and the parameters (3.10), (3.11), and (4.2). The modulus $\mu(z, \lambda = -1)$ increases monotonically with z, approaching a finite limit value $\mu_\infty \approx 47.36$. (For scaling exponents $\lambda < -1$, the modulus attains a maximum at finite z, and it diverges for $\lambda > -1$.) If μ is calculated by substitution of the ascending series (4.10) and (4.15), there is virtually no difference with the exact modulus for redshifts up to $z \approx 2.2$, as long as we stay in the Euclidean regime, $\hat{R} \geq 10$. In this redshift range, the fit is not sensitive to curvature radii above $\hat{R} = 10$, that is, indistinguishable from the Euclidean limit $\hat{R} \to \infty$, and it only provides a test of the low-z evolution. The fit in Fig. 1 is done with $\hat{R} = 10$. The luminosity scales with the synthesized ^{56}Ni mass, which scatters from SN to SN by up to a factor of ten and is age dependent (Stritzinger et al. 2006a, 2006b). Therefore, it is prudent to adopt an approach independent of progenitor models, the linear scaling $L \propto h(z)$ being inferred from an empirical fit. Further evidence for a luminosity dependence of Type Ia supernovae on look-back time is given in Gallagher et al. (2008), where a metallicity correction of the SN Ia Hubble diagram is suggested.

4.3 Low-z expansion of comoving volume and Hubble parameter

The leading orders of the ascending D/R-series of the comoving hyperbolic volume $V(D)$ in (2.20) read

$$V(D) = \frac{4\pi}{3} D^3 \left(1 + \frac{1}{5}\left(\frac{D}{R}\right)^2 + \mathrm{O}\left(D^4\right)\right). \tag{4.11}$$

We substitute the series expansion of $D(z)$ in (4.7) to obtain

$$V(z) = \frac{4\pi}{3}\left(\frac{c}{H_0} z\right)^3 \left(1 - \frac{3}{2}\varepsilon z + \left(\frac{1}{5\hat{R}^2} - \frac{\delta}{2} - \varepsilon + \frac{9}{4}\varepsilon^2\right) z^2 + \mathrm{O}\left(z^3\right)\right). \tag{4.12}$$

The constants ε and δ in (4.2) give

$$V(z) = \frac{4\pi}{3}\left(\frac{c}{H_0}\right)^3 z^3 \left(1 + 4.18 \times 10^{-3} z + \left(\frac{1}{5\hat{R}^2} - 0.209\right) z^2 + \cdots\right). \tag{4.13}$$

To obtain the volume at emission time, we have to multiply by $a^3(\tau_1) = (1+z)^{-3}$, see the text after (2.20).

We turn to the low-z expansion of the Hubble parameter. In the limit $\tau \to \tau_0$, we expand $H = \dot{a}(\tau)/a(\tau)$ in $\Delta = H_0 \cdot (\tau - \tau_0)$, by making use of (2.2) and (4.5):

$$\frac{H^\lambda(\tau)}{H_0^\lambda} = 1 - \varepsilon\lambda\Delta + \frac{\lambda}{2}\left(\delta + 3\varepsilon + (\lambda - 1)\varepsilon^2\right)\Delta^2 + \cdots, \tag{4.14}$$

where λ is an arbitrary real exponent. The constants ε and δ are defined in (2.9) and (2.10). Replacing Δ by the low-z expansion of the look-back interval Δ_1 in (4.4), we arrive at

$$h^\lambda(z) = 1 + \lambda\varepsilon z + \lambda\left(\frac{\delta}{2} + \varepsilon + \frac{\lambda - 2}{2}\varepsilon^2\right) z^2 + \cdots, \tag{4.15}$$

where $h(z) = H(\tau_1(z))/H_0$ is the rescaled Hubble parameter coinciding with the normalized gravitational constant $G(\tau_1(z))/G_0$, see (2.4). The constants (4.2) give

$$h(z) = 1 - 2.79 \times 10^{-3} z + 0.209 z^2 + \cdots, \tag{4.16}$$

as well as $\dot{H}_0/H_0 \approx 1.938 \times 10^{-4}$ Gyr^{-1} and $\ddot{H}_0/H_0 \approx 2.014 \times 10^{-3}$ Gyr^{-2}, see (4.14), to be compared to the bounds $(2 \pm 7) \times 10^{-4}$ Gyr^{-1} and $(4 \pm 5) \times 10^3$ Gyr^{-2} from lunar laser ranging (Müller and Biskupek 2007).

5 Evolution of the AGN space density based on constant dimensionless ratios and a varying gravitational constant

5.1 Hubble parameter as universal scaling variable for redshift evolution: count-redshift relation

A moderate dimensionless ratio,

$$\Omega_\mathrm{m} := \frac{8\pi}{3}\frac{G_0\rho_\mathrm{m}(\tau_0)}{H_0^2} \approx 0.3 \pm 0.1, \tag{5.1}$$

can be composed with the mass density ρ_m of the universe (Kowalski et al. 2008; Komatsu et al. 2009). This ratio is kept constant in the cosmic evolution, $G(\tau)\rho_\mathrm{m}(\tau) \propto H^2(\tau)$. Since the rest mass does not vary in cosmic time, the comoving number density scales as $\rho(\tau) \propto H(\tau)$, see the text after (2.4). This is a crucial departure from the conservation law $\rho(\tau) \propto 1$, implying a conserved number count $\mathrm{d}N = \rho\,\mathrm{d}V$, where $\mathrm{d}V$ is the differential comoving volume (2.20).

We consider a luminosity-dependent number density, using the ansatz

$$\rho(z, L) := \rho_0 h^{1+\delta}(z) F\left(L h^\lambda(z)\right), \tag{5.2}$$

where the factor $\rho_0 h^{1+\delta}(z)$ accounts for density evolution, by source creation and destruction for instance. The scaling variables in (5.2) are powers of the Hubble parameter $h(z) = H(\tau_1(z))/H_0$, see (2.18). A constant Ω_m suggests $\delta = 0$ in (5.2), but we leave the choice of the exponents open at this stage. The factor $F(Lh^\lambda(z))$ accounts for the luminosity evolution, where the scaling function

$$F(L_0) := \int_{L_0/L_\mathrm{c}}^\infty y^{\mu-1}(1+y)^\nu \mathrm{e}^{-\kappa y}\,\mathrm{d}y = U(\mu, \nu, \kappa; L_0/L_\mathrm{c}) \tag{5.3}$$

is composed of a power law $y^{\mu-1}$ at faint luminosities, and a power law with exponential cutoff $y^{\mu+\nu-1}\mathrm{e}^{-\kappa y}$ at the bright end. $F(L_0)$ is parametrized by the luminosity scale L_c and exponents μ, ν, and $\kappa > 0$. Some limit cases of the incomplete confluent function U defined by (5.3) are outlined after (5.21). (Exponent δ in (5.2) is not to be confused with coefficient (2.10) in the ascending series of the expansion factor, and exponent μ in (5.3) is unrelated to the distance modulus.)

The differential number count is assembled as

$$\mathrm{d}N(z, L) = \rho(z, L) V'(z)\,\mathrm{d}z, \tag{5.4}$$

where $\mathrm{d}V(z) = \mathrm{area}(D)\,\mathrm{d}D(z)$ is the comoving volume element, see (2.18)–(2.20), so that

$$V'(z) = \frac{c^3}{H_0^3}\frac{4\pi\hat{R}^2}{h(z)}\sinh^2\frac{D(z)}{R}. \tag{5.5}$$

We find the differential and cumulative counting functions as

$$N'(z,L)=\rho(z,L)V'(z),$$
$$N(z,L)=\int_0^z N'(z,L)\,\mathrm{d}z, \tag{5.6}$$

with ρ in (5.2) and V' in (5.5).

5.2 Luminosity function and comoving AGN/QSO space density

The luminosity function $\Phi(z,L)$ is defined as source count per unit luminosity and unit volume (Croom et al. 2004; Miyaji et al. 2001; Silverman et al. 2008; Ueda et al. 2003),

$$N(z,L)=\int_0^z\int_L^\infty \Phi(z,L)\,\mathrm{d}L\,\mathrm{d}V(z), \tag{5.7}$$

so that the comoving space density $\rho(z,L)$ can be identified with the cumulative luminosity function

$$\rho(z,L)=\frac{\mathrm{d}N}{\mathrm{d}V}=\int_L^\infty \Phi(z,L)\,\mathrm{d}L. \tag{5.8}$$

We find, by comparing to (5.2) and (5.3),

$$\Phi(z,L)=-\frac{\mathrm{d}\rho(z,L)}{\mathrm{d}L}=\rho_0 h^{1+\delta+\lambda}(z)\,f\big(Lh^\lambda(z)\big), \tag{5.9}$$

$$f(L_0):=-F'(L_0)=\frac{1}{L_\mathrm{c}}(L_0/L_\mathrm{c})^{\mu-1}(1+L_0/L_\mathrm{c})^\nu \times\exp(-\kappa L_0/L_\mathrm{c}). \tag{5.10}$$

The space density and luminosity function are thus related to the scaling function (5.3) by

$$\rho(z,L)=\frac{N'(z,L)}{V'(z)}=\rho_0 h^{1+\delta}U\big(\mu,\nu,\kappa;Lh^\lambda/L_\mathrm{c}\big), \tag{5.11}$$

$$\Phi(z,L)=\frac{\rho_0}{L_\mathrm{c}}h^{1+\delta+\lambda}\big(Lh^\lambda/L_\mathrm{c}\big)^{\mu-1}\big(1+Lh^\lambda/L_\mathrm{c}\big)^\nu \times\exp\big(-\kappa Lh^\lambda/L_\mathrm{c}\big). \tag{5.12}$$

The redshift dependence is exclusively via the Hubble parameter $h(z)$. The space density differs from the differential count by the volume factor (5.5), $\mathrm{d}N(z,L)/\mathrm{d}z=\rho(z,L)V'(z)$. We may introduce $\log(L/L_\mathrm{c})$ or the absolute magnitude, $M-M_0=-(5/2)\log(L/L_\mathrm{c})$, as integration variable in (5.8),

$$\rho(z,L)=\int_{\log(L/L_\mathrm{c})}^\infty \hat\Phi\big(z,L_\mathrm{c}\cdot 10^x\big)\,\mathrm{d}x, \tag{5.13}$$

with the rescaled luminosity function

$$\hat\Phi(z,L):=-\frac{\mathrm{d}\rho(z,L)}{\mathrm{d}\log(L/L_\mathrm{c})}=\frac{L\Phi(z,L)}{\log\mathrm{e}}. \tag{5.14}$$

Returning to (5.8), we find the comoving space density in a finite luminosity interval (L,L_max) as

$$\begin{aligned}\rho(z;L,L_\mathrm{max})&=\int_L^{L_\mathrm{max}}\Phi(z,L)\,\mathrm{d}L=\rho(z,L)-\rho(z,L_\mathrm{max})\\&=\rho_0 h^{1+\delta}\int_{Lh^\lambda/L_\mathrm{c}}^{L_\mathrm{max}h^\lambda/L_\mathrm{c}} y^{\mu-1}(1+y)^\nu\exp(-\kappa y)\,\mathrm{d}y\\&=\rho_0 h^{1+\delta+\lambda\mu}\frac{L^\mu}{L_\mathrm{c}^\mu}\int_1^{L_\mathrm{max}/L}x^{\mu-1}\bigg(1+\frac{Lh^\lambda}{L_\mathrm{c}}x\bigg)^\nu\\&\quad\times\exp\bigg(-\kappa\frac{Lh^\lambda}{L_\mathrm{c}}x\bigg)\,\mathrm{d}x.\end{aligned} \tag{5.15}$$

Density $\rho(z;L)$ in (5.8) and (5.11) is recovered in the limit $L_\mathrm{max}\to\infty$. We briefly discuss the qualitative redshift scaling of $\rho(z;L,L_\mathrm{max})$. If $L/L_\mathrm{c}\ll 1$ and $\kappa\ll 1$ as well as $\lambda>0$, we have roughly $\rho\propto h^{1+\delta+\lambda\mu}$, up to a redshift z_c1 defined by $h^\lambda(z_\mathrm{c1})\approx L_\mathrm{c}/L$. Exponential decay, $\rho\propto\exp(-\kappa Lh^\lambda/L_\mathrm{c})$, sets in at about z_c2 defined by $h^\lambda(z_\mathrm{c2})\approx L_\mathrm{c}/(L\kappa)$. In between, there is a power-law crossover $\rho\propto h^{1+\delta+\lambda(\mu+\nu)}$. The typical case is $\mu>0$ and $\mu+\nu<0$, so that the first power law with large positive exponent $1+\delta+\lambda\mu$ corresponds to a rapid increase up to z_c1. This is followed by a power law $\propto h^{1+\delta+\lambda(\mu+\nu)}$ with negative exponent implying power-law decay up to z_c2, where exponential decay sets in.

The fit of the AGN space density in Fig. 2 is performed with $\rho(z;L,L_\mathrm{max})$ in (5.15). It is convenient to use a dimensionless density scale $\hat\rho(L,L_\mathrm{max})$ defined by $\rho(0;L,L_\mathrm{max})=\hat\rho H_0^3/c^3$, to be substituted for ρ_0 in (5.15),

$$\rho_0\big[\mathrm{Mpc}^{-3}\big]\approx\frac{1.1680\times10^{-11}\hat\rho}{\int_{L/L_\mathrm{c}}^{L_\mathrm{max}/L_\mathrm{c}}y^{\mu-1}(1+y)^\nu\mathrm{e}^{-\kappa y}\,\mathrm{d}y}. \tag{5.16}$$

Here, $H_0^3/c^3\approx1.1680\times10^{-11}$ Mpc^{-3}, see the text after (2.4). We adopt the X-ray luminosity scale used in Hasinger et al. (2005), writing L_{44} for L in units of 10^{44} erg/s, and analogously $L_{\mathrm{c},44}$. The expansion factor is specified in (3.10) and (3.11). We consider the luminosity interval $L_{44}=1$, $L_{\mathrm{max},44}=10$, and use the exponents $\mu=2$ and $\nu=-5/2$, as well as $\delta=0$ and $\lambda=6$ as input parameters. The fitting parameters are $\hat\rho(L,L_\mathrm{max})\approx 9.0\times10^3$, $L_{\mathrm{c},44}(L,L_\mathrm{max})\approx40$, and $\kappa\approx1.6\times10^{-5}$, so that $\rho_0\approx5.0\times10^{-6}$ Mpc^{-3}, see (5.16). The rapid rise of the AGN space density in Fig. 2 is due to the large exponent $1+\delta+\lambda\mu$; see the discussion following (5.15).

When studying source counts in Sect. 6, we will need the redshift asymptotics of the luminosity function (5.12) and the space density (5.11). Their high-z limit, $h^\lambda(z)\to\infty$, reads

$$\Phi(z\to\infty,L)\sim\frac{\rho_0}{L_\mathrm{c}}h^{1+\delta+\lambda}\big(Lh^\lambda/L_\mathrm{c}\big)^{\mu+\nu-1}\times\exp\big(-\kappa Lh^\lambda/L_\mathrm{c}\big),\tag{5.17}$$

$$\rho(z\to\infty,L)\sim\frac{L_\mathrm{c}}{\kappa h^\lambda}\Phi(z,L).\tag{5.18}$$

This is also valid at fixed z for $L\to\infty$. We will also need the asymptotic redshift derivative of the comoving volume, see (3.7) and (5.5),

$$V'(z\to\infty)\sim4\pi\frac{c^3}{H_0^3}\frac{\hat R^2\sinh^2 D_\infty}{h(z)}.\tag{5.19}$$

In the low-z regime, $h(z)\to1$, we find that, see (4.12), (5.2), and (5.3),

$$\begin{aligned}&\rho(z\to0,L)\sim\rho_0F(L),\\&V'(z\to0)\sim4\pi\frac{c^3}{H_0^3}z^2.\end{aligned}\tag{5.20}$$

The high- and low-z asymptotics of the differential counting function, $N'(z,L)=\rho(z,L)V'(z)$, follows accordingly.

We list some properties and special cases of the scaling function (5.3),

$$U(\mu,\nu,\kappa;y):=\int_y^\infty y^{\mu-1}(1+y)^\nu\mathrm{e}^{-\kappa y}\,\mathrm{d}y.\tag{5.21}$$

First, $U(\mu,\nu,\kappa;0)=\Gamma(\mu)U(\mu,1+\mu+\nu,\kappa)$, where $U(a,b,z)$ is the confluent hypergeometric function (Magnus et al. 1966), and $\mu>0$ is required for convergence at $y=0$. (We use the same symbol U for the incomplete confluent function (5.21), with one more argument.) Otherwise, if $\mu<0$, we find $U(\mu,\nu,\kappa;y\to0)\sim-y^\mu/\mu$. The $y\to\infty$ limit is $U(\mu,\nu,\kappa;y)\sim y^{\mu+\nu-1}\mathrm{e}^{-\kappa y}/\kappa$, and the y derivative of (5.21) reads $U'=-y^{\mu-1}(1+y)^\nu\mathrm{e}^{-\kappa y}$. Apparently, $U(\mu,\nu,\kappa;y)$ is elementary for positive integer exponents μ and ν. At $\nu=0$, we recover the cumulative Schechter luminosity function $U(\mu,0,\kappa;y)=\kappa^{-\mu}\Gamma(\mu,\kappa y)$, see, e.g., Babbedge et al. (2006). A positive integer exponent ν thus amounts to a linear combination of incomplete gamma functions. A negative ν gives luminosity functions similar to reciprocal linear combinations of two power laws as used in Croom et al. (2004), Miyaji et al. (2001), and Ueda et al. (2003), apart from the exponential cutoff. At $\mu=1$, we find $U(1,\nu,\kappa;y)=\kappa^{-\nu-1}\mathrm{e}^\kappa\Gamma(1+\nu,(1+y)\kappa)$, where the incomplete gamma function can be reduced to the exponential integral in the case of integer ν, and to the error function for half-integer ν; a positive integer exponent μ can be dealt with by multiple κ differentiation, according to (5.21).

6 Flux-limited source counts and luminosity evolution

6.1 Flux parametrization of the counting function

To derive the flux-limited count, that is, the number $N(S)$ of sources exceeding a lower flux threshold S, we start with the counting function $N'(z,L)$ in (5.6). The flux parametrization is done by replacing the intrinsic luminosity L by the apparent flux, via the flux-redshift relation (2.24),

$$L(z,S)=4\pi R^2\sigma_D(z)S,\tag{6.1}$$

$$\sigma_D(z):=(1+z)^{s+1}\sinh^2\frac{D(z)}{R},\tag{6.2}$$

where $D(z)$ is the comoving distance defined in (2.18) or (3.4) and s is the spectral index. The flux-limited count cumulative in redshift reads, see (5.6) and (5.7),

$$\begin{aligned}N(S)&=\int_\varepsilon^\infty N'\big(z,L(z,S)\big)\,\mathrm{d}z\\&=\int_S^\infty\int_\varepsilon^\infty n(z,S)\,\mathrm{d}z\mathrm{d}S,\end{aligned}\tag{6.3}$$

where we have introduced a lower cutoff ε in the redshift integration to allow the interchange of integrations. (This cutoff ε is not to be confused with coefficient (2.9) in the ascending series of the expansion factor.) Density $n(z,S)$ is related to the counting function by

$$\begin{aligned}N'\big(z,L(z,S)\big)&=\int_S^\infty n(z,S)\,\mathrm{d}S\\&=\rho\big(z,L(z,S)\big)V'(z),\end{aligned}\tag{6.4}$$

where ρ is the flux-parametrized space density (5.8),

$$\rho\big(z,L(z,S)\big)=4\pi R^2\sigma_D(z)\int_S^\infty\Phi\big(z,L(z,S)\big)\,\mathrm{d}S.\tag{6.5}$$

This allows us to identify

$$n(z,S)=4\pi R^2\sigma_D(z)\Phi\big(z,L(z,S)\big)V'(z),\tag{6.6}$$

where the flux-parametrized luminosity function (5.9) reads

$$\Phi\big(z,L(z,S)\big)=\rho_0h^{1+\delta+\lambda}(z)f\big(L(z,S)h^\lambda(z)\big).\tag{6.7}$$

The scaling function $f(Lh^\lambda)$ is assembled from (5.10) and (6.1),

$$f(Lh^\lambda)=\frac{1}{4\pi R^2S_\mathrm{c}}\left(g(z)\frac{S}{S_\mathrm{c}}\right)^{\mu-1}\left(1+g(z)\frac{S}{S_\mathrm{c}}\right)^\nu\times\exp\left(-\kappa g(z)\frac{S}{S_\mathrm{c}}\right),\tag{6.8}$$

where we have introduced the shortcuts

$$\begin{aligned}&g(z):=\sigma_D(z)h^\lambda(z),\\&S_\mathrm{c}:=\frac{L_\mathrm{c}}{4\pi R^2}=\frac{L_\mathrm{c}H_0^2}{4\pi c^2}\frac{1}{\hat R^2}.\end{aligned}\tag{6.9}$$

To obtain the asymptotic limits of $\Phi(z,L(z,S))$ and $\rho(z,L(z,S))$, valid for $g(z)\to\infty$ as well as $S\to\infty$, we

only need to substitute identity $h^\lambda L/L_c = gS/S_c$ into (5.17) and (5.18), and set $L_c = 4\pi R^2 S_c$.

We may write density (6.5) as, see (5.2),

$$\rho\big(z, L(z,S)\big) = \rho_0 h^{1+\delta}(z) F\big(L(z,S)h^\lambda(z)\big), \tag{6.10}$$

with the scaling function, see (5.3) and (5.21),

$$\begin{aligned} F\big(Lh^\lambda\big) &= \int_{gS/S_c}^\infty y^{\mu-1}(1+y)^\nu \mathrm{e}^{-\kappa y}\,\mathrm{d}y \\ &= U(\mu,\nu,\kappa; gS/S_c). \end{aligned} \tag{6.11}$$

If $\mu > 0$, this admits a finite limit at $S = 0$, see the text after (5.21),

$$F(0) = \Gamma(\mu) U(\mu, 1+\mu+\nu, \kappa). \tag{6.12}$$

In the absence of a lower flux threshold, we thus find the redshift scaling $\rho(z,0) \propto h^{1+\delta}(z)$ at $S = 0$. If $\mu < 0$, the scaling $F(Lh^\lambda) \sim -(g(z)S/S_c)^\mu/\mu$ holds for $g(z)S \to 0$. The total count, $N_\infty := N(S=0)$, can be assembled from (6.3), (6.4), (6.10), and (6.12),

$$N_\infty = \int_\varepsilon^\infty N'(z,0)\,\mathrm{d}z, \quad N'(z,0) = \rho_0 F(0) h^{1+\delta}(z) V'(z). \tag{6.13}$$

To obtain the high-z asymptotics of the integrand $N'(z,0)$, we substitute $h(z) \sim h_\infty(1+z)^n$, see (3.14) (where $n > 1$, see the text after (3.6)), as well as the asymptotic $V'(z\to\infty)$ in (5.19),

$$\begin{aligned} &N'(z\to\infty,0) \sim \hat\rho_0 n_z (1+z)^{\xi-1}, \quad \xi := n\delta + 1, \\ &n_z := 4\pi \hat R^2 F(0) h_\infty^\delta \sinh^2 D_\infty, \hat\rho_0 := \rho_0 c^3/H_0^3. \end{aligned} \tag{6.14}$$

The amplitude h_∞ is defined in (3.15). Thus, $\xi < 0$ is the condition for N_∞ to be finite, in addition to $\mu > 0$, see the text after (6.11). The low-z scaling is $N'(z\to 0,0) \sim 4\pi\hat\rho_0 F(0) z^2$, obtained via $h(z) \sim 1$, see (4.15), and the asymptotic $V'(z\to 0)$ in (5.20).

When comparing to observational plots, it is sometimes convenient to replace the flux variable S by the apparent magnitude $m - m_0 = -(5/2)\log(S/S_c)$. That is, the foregoing relations can be parametrized in apparent and absolute magnitudes (as defined before (5.13)) instead of apparent flux and intrinsic luminosity. In this case, we use the logarithmic version of the flux–redshift relation (6.1), the magnitude–redshift relation

$$m - m_0 = M - M_0 + \frac{5}{2}\log\sigma_D(z), \tag{6.15}$$

with σ_D defined in (6.2).

6.2 Scaling exponents of differential and cumulative counts

To derive the high- and low-S asymptotics of the cumulative count $N(S)$ in (6.3), we start with the derivative

$$\begin{aligned} n(S) &:= -N'(S) = \int_\varepsilon^\infty n(z,S)\,\mathrm{d}z, \\ N(S) &= \int_S^\infty n(S)\,\mathrm{d}S, \end{aligned} \tag{6.16}$$

where the integrand $n(z,S)$ is assembled from (6.6)–(6.9),

$$\begin{aligned} n(z,S) = \frac{\rho_0}{S_c} h^{1+\delta}(z) g^\mu(z) V'(z) (S/S_c)^{\mu-1} \\ \times (1+gS/S_c)^\nu \exp(-\kappa g S/S_c). \end{aligned} \tag{6.17}$$

In the following, we derive the leading-order asymptotics of $n(S)$ in (6.16); the scaling exponents of the cumulative count are found by integration of the asymptotic $n(S)$.

6.2.1 High-flux asymptotics

The high-S scaling of the differential count $n(S)$ in (6.16) is determined by small z, provided that $g(z)$ is monotonically increasing, see (6.17). It can also happen that $g(z)$ reaches a maximum and decreases to zero for $z\to\infty$; this case is discussed after (6.20). By expanding the integrand $n(z,S)$ at $z = \varepsilon$, we find

$$\begin{aligned} n(S\to\infty) &\sim \frac{\rho_0}{\kappa S_c} h^{1+\delta}(\varepsilon) g^{\mu+\nu}(\varepsilon) \frac{V'(\varepsilon)}{g'(\varepsilon)} \\ &\quad \times (S/S_c)^{\mu+\nu-2} \exp\left(-\kappa g(\varepsilon)\frac{S}{S_c}\right), \\ N(S\to\infty) &\sim \frac{S_c}{\kappa g(\varepsilon)} n(S). \end{aligned} \tag{6.18}$$

The derivative $g'(\varepsilon)$ of the scaling function (6.9) is calculated by making use of (2.17) and (2.18). This exponential decay is in strong contrast to the power-law decay at $\varepsilon = 0$, which is determined by the low-z asymptotics of density $n(z,S)$. To recover this Euclidean limit, we return to (6.17) and substitute $h(z) \sim 1$, see (4.15), $g(z) \sim \sigma_D(z) \sim z^2/\hat R^2$, see (4.9), (6.2), and (6.9), as well as $V'(z\to 0)$, see (5.20),

$$\begin{aligned} n(z\to 0, S) &\sim 4\pi\hat\rho_0 \frac{z^{2\mu+2}}{\hat R^{2\mu}} \frac{S^{\mu-1}}{S_c^\mu} \left(1 + \frac{z^2}{\hat R^2}\frac{S}{S_c}\right)^\nu \\ &\quad \times \exp\left(-\kappa \frac{z^2}{\hat R^2}\frac{S}{S_c}\right). \end{aligned} \tag{6.19}$$

Here, we have defined $\rho_0 =: \hat\rho_0 H_0^3/c^3$, measuring density (5.2) in units of H_0^3/c^3, analogously to the curvature radius $R = \hat R c/H_0$, see (2.18). Apparently, $\mu > -3/2$ is required for the convergence of integral (6.16) at $\varepsilon = 0$. We substitute

(6.19) into (6.16), set $\varepsilon = 0$, and carry out the z integration according to (5.21) (with $y = 0$), to find the Euclidean high-S scaling

$$n(S \to \infty) \sim \hat{\rho}_0 n_\infty \frac{S_c^{3/2}}{S^{5/2}}, \qquad N(S \to \infty) \sim \frac{2}{3} \hat{\rho}_0 n_\infty \frac{S_c^{3/2}}{S^{3/2}},$$
$$n_\infty := 2\pi \hat{R}^3 \Gamma\left(\mu + \frac{3}{2}\right) U\left(\mu + \frac{3}{2}, \mu + \nu + \frac{5}{2}, \kappa\right). \tag{6.20}$$

As mentioned, the scale factor $g(z)$ in the exponent of $n(z, S)$ in (6.17) can be decreasing for high z. The high-z limit of $g(z)$ in (6.9) is readily assembled from $\sigma_D(z) \sim z^{s+1} \sinh^2 D_\infty$, see (3.7) and (6.2), as well as $h(z) \sim h_\infty z^n$, see (3.14), and $V'(z \to \infty)$ in (5.19),

$$g(z \to \infty) \sim h_\infty^\lambda z^\chi \sinh^2 D_\infty, \quad \chi := n\lambda + s + 1. \tag{6.21}$$

This decreases to zero if exponent χ is negative. We substitute these limits into (6.17), to obtain the high-z counterpart to (6.19),

$$n(z \to \infty, S) \sim \hat{A} \hat{S}^{\mu-1} z^{\varphi-1} \left(1 + \hat{S} z^\chi\right)^\nu \exp\left(-\kappa \hat{S} z^\chi\right),$$
$$\varphi := \xi + \chi\mu, \hat{A} := 4\pi \hat{\rho}_0 \frac{\hat{R}^2}{S_c} h_\infty^{\delta+\lambda} \sinh^4 D_\infty,$$
$$\hat{S} := \frac{S}{S_c} h_\infty^\lambda \sinh^2 D_\infty. \tag{6.22}$$

Here, $\xi = n\delta + 1$, as in (6.14). If $\chi < 0$, then $\varphi < 0$ is necessary for integral (6.16) to converge, in addition to condition $\mu > -3/2$ required at low z to define the differential count $n(S)$ at $\varepsilon = 0$. On substituting (6.22) into (6.16), we find the high-S scaling

$$n(S) \sim \frac{\hat{A}}{|\chi|} \Gamma\left(\frac{\varphi}{\chi}\right) U\left(\frac{\varphi}{\chi}, \frac{\varphi}{\chi} + \nu + 1, \kappa\right) \frac{1}{\hat{S}^{\sigma+1}},$$
$$\sigma := \frac{\xi}{\chi} = \frac{n\delta + 1}{n\lambda + s + 1}, \ \varphi = \chi(\sigma + \mu). \tag{6.23}$$

Here, $\chi < 0$ as well as $\varphi < 0$ is implied. The cutoff ε in (6.16) does not enter in leading order. The exponents δ and λ determine the redshift scaling of the number density in (5.2). The exponent $n = 1/\gamma$ is defined by the space expansion, see the text after (2.7), and s is the spectral index in the flux-redshift relation, see (2.24) and (6.2). We assume a positive exponent σ in (6.23); otherwise, the cumulative count $N(S)$ is not defined for $\chi < 0$. The asymptotic $N(S \to \infty)$ is obtained by substituting (6.23) into (6.16),

$$n(S) \sim \hat{\rho}_0 n_0 \frac{S_c^\sigma}{S^{\sigma+1}}, \qquad N(S) \sim \frac{\hat{\rho}_0 n_0}{\sigma} \frac{S_c^\sigma}{S^\sigma},$$
$$n_0 := 4\pi \hat{R}^2 h_\infty^{\delta-\lambda\sigma} \frac{\sinh^{2(1-\sigma)} D_\infty}{|\chi|} \Gamma(\sigma + \mu) \tag{6.24}$$
$$\times U(\sigma + \mu, \sigma + \mu + \nu + 1, \kappa).$$

Accordingly, if $0 < \sigma < 3/2$ (and $\chi < 0$), we find the scaling $N(S \to \infty) \propto S^{-\sigma}$, which overpowers the Euclidean limit (6.20). If $\sigma = 3/2$, the $S \to \infty$ asymptotics of $N(S)$ is obtained by adding the low- and high-z contributions (6.20) and (6.24); the latter only exists for $\chi < 0$. If $\sigma > 3/2$, the Euclidean high-S scaling (6.20) remains valid even for negative χ, as it dominates the high-z contribution (6.24). A finite cutoff ε turns the Euclidean scaling (6.20) into exponential decay (6.18), so that the power law (6.24) (which exists only if $\chi < 0$) also applies for $\sigma > 3/2$. If χ is positive, the $S \to \infty$ asymptotics is either exponential or Euclidean, according to (6.18) and (6.20).

6.2.2 *Power-law scaling in the low-flux regime*

To derive the low-S scaling of the differential count $n(S)$, we split integral (6.16) into

$$n(S) = I_0 + I_\infty,$$
$$I_0 := \int_\varepsilon^\Lambda n(z, S)\, \mathrm{d}z, \ I_\infty := \int_\Lambda^\infty n(z, S)\, \mathrm{d}z, \tag{6.25}$$

where Λ is a large cutoff parameter, so that the high-z limit (6.22) of $n(z, S)$ can be substituted into I_∞. If the exponents χ and φ (defined in (6.21) and (6.22)) are positive, we can carry out the integration I_∞ as in (6.23), to find $I_\infty \sim n_0 S_c^\sigma / S^{\sigma+1}$, with exponent σ defined in (6.23) and amplitude n_0 in (6.24). (In leading order, I_∞ does not depend on the cutoff parameter Λ.) Regarding the exponents, we note $\varphi = \chi(\sigma + \mu)$, see (6.23), which implies $\sigma > -\mu$, as χ and φ have the same sign. As for integral I_0 in (6.25), we substitute density $n(z, S)$ as stated in (6.17), and perform the limit $S \to 0$ in the ν dependent factor and the exponential, so that $I_0 \propto S^{\mu-1}$, with a Λ dependent proportionality factor (which diverges for $\Lambda \to \infty$). Since $\sigma > -\mu$, the leading-order asymptotics of $n(S)$ is determined by I_∞. Accordingly, if $\chi > 0$ and $\varphi > 0$, the low-S scaling of the differential and cumulative counts is given by (6.24), now applicable for $S \to 0$.

The scaling of $N(S)$ stated in (6.24) is valid only if $\sigma > 0$. A negative exponent σ is admissible for $\chi > 0$, and implies a negative $\xi = \chi\sigma$, see (6.23). A negative σ also implies $\mu > 0$, since $\sigma > -\mu$. Therefore, if $\sigma < 0$, we obtain a finite limit, $N(S \to 0) = N_\infty$, as $\mu > 0$ and $\xi < 0$ are the conditions for $N(S \to 0)$ to be finite, see (6.14). The numerical calculation of the total count N_∞ is indicated after (6.32).

Next we study the low-S scaling of $n(S)$ for negative exponents χ and φ. On substituting the high-z expansion (6.22) into I_∞, we find $I_\infty \propto S^{\mu-1}$, with an amplitude vanishing for $\Lambda \to \infty$. As for integral I_0 in (6.25), we perform the same procedure as above, and find $I_0 \propto S^{\mu-1}$, with a Λ dependent proportionality factor converging to a finite limit

for $\Lambda \to \infty$. The low-S asymptotics is thus determined by I_0, which gives, for $\chi < 0$ and $\varphi < 0$,

$$n(S \to 0) \sim \hat{\rho}_0 n_1 \frac{S^{\mu-1}}{S_c^{\mu}}, \qquad N(S \to 0) \sim \frac{\hat{\rho}_0 n_1}{|\mu|} \frac{S^{\mu}}{S_c^{\mu}}, \qquad n_1 := \frac{H_0^3}{c^3} \int_{\varepsilon}^{\infty} h^{1+\delta}(z) g^{\mu}(z) V'(z)\, \mathrm{d}z, \tag{6.26}$$

with $V'(z)$ in (5.5). The amplitude n_1 is calculated by using the emission time as integration variable, see the text after (6.32). The indicated scaling of $N(S)$ only holds for negative μ, as the cumulative count admits a finite limit for $\mu > 0$, $N(S \to 0) = N_\infty$. In fact, as mentioned after (6.23), we can assume a positive σ if $\chi < 0$; otherwise, $N(S)$ is not defined, see (6.16) and $n(S)$ in (6.24). A positive σ implies $\xi < 0$, since $\chi < 0$, see (6.23). If in addition $\mu > 0$, this results in a finite N_∞, according to (6.13) and (6.14). In contrast, a negative μ implies the scaling (6.26) for $N(S \to 0)$. Finally, if $\varepsilon = 0$, $N(S)$ cannot decrease faster than $S^{-3/2}$, since condition $\mu > -3/2$ is necessary for the convergence of the integrals in (6.16) and (6.26) defining the differential count $n(S)$, see the text after (6.19).

It remains to settle the low-S asymptotics of $n(S)$ for the case $\chi > 0$ and $\varphi < 0$, so that $\sigma < -\mu$, see the text after (6.25). (The combination $\chi < 0$ and $\varphi > 0$ need not be considered, since $n(S)$ is ill defined in this case, see the text after (6.22).) Performing the same procedure as above, we find that $I_\infty \propto S^{\mu-1}$ with an amplitude vanishing for $\Lambda \to \infty$, as well as $I_0 \propto S^{\mu-1}$ with a proportionality factor that stays finite for $\Lambda \to \infty$ since $\varphi < 0$ in (6.22). Thus we recover $n(S \to 0)$ in (6.26). As for the cumulative count $N(S \to 0)$, we find, for $\mu > 0$, a finite limit N_∞, see (6.13), since σ is negative, $\sigma < -\mu$, and so is $\xi = \chi\sigma$. In the case of a negative exponent μ, $N(S)$ scales as stated in (6.26).

6.3 Crossover from high to low flux limits: number count of soft X-ray point sources

In the intermediate regime, at moderate flux limit S, we have to numerically integrate the source count $N(S)$ in (6.3), whose integrand is assembled from (6.4), (6.10), and (6.11),

$$N'\big(z, L(z,S)\big) = \rho_0 h^{1+\delta}(z) U\big(\mu, \nu, \kappa; g(z)S/S_c\big) V'(z), \tag{6.27}$$

with $V'(z)$ in (5.5). We introduce the emission time as integration variable instead of z, by virtue of $1 + z = 1/a(\tau_1)$, see (2.14). The differential required in the reparametrization is $\mathrm{d}z = -H(\tau_1)\mathrm{d}\tau_1/a(\tau_1)$, see (2.15). It is convenient to use a rescaled dimensionless time variable in units of the present epoch, $0 \le y \le 1$, $\tau_1 = \tau_0 y$, to write the cumulative count (6.3) as, see (5.5) and (6.27),

$$N(S) = 4\pi \hat{\rho}_0 \hat{R}^2 H_0 \tau_0 \int_0^{\tau_1(\varepsilon)/\tau_0} \frac{\mathrm{d}y}{a(y)} h^{1+\delta}(y) \times U\big(\mu, \nu, \kappa; g(y)S/S_c\big) \sinh^2 \frac{D(y)}{R}. \tag{6.28}$$

Here, $\hat{\rho}_0$ and $\hat{R}$ denote the dimensionless density scale and the curvature radius in units of H_0^3/c^3 and c/H_0, respectively, see the text after (6.19). The upper integration boundary $\tau_1(\varepsilon)/\tau_0$ is obtained by numerical inversion of (3.1) at $z = \varepsilon$. By employing emission time as integration variable, we need to invert this equation only once, at the integration boundary.

We summarize the quantities occurring in the integrand of $N(S)$ in (6.28). U is the incomplete confluent function (5.21). The expansion factor $a(y)$ and the normalized Hubble parameter $h(y) = H(y)/H_0$ read, see (2.6) and (2.7),

$$a(y) = y^{\beta} \frac{\sinh^{\alpha}(\eta y)}{\sinh^{\alpha}\eta}, \qquad h(y) = \frac{1}{H_0\tau_0}\left(\alpha\eta \coth(\eta y) + \frac{\beta}{y}\right). \tag{6.29}$$

The comoving distance in the argument of the hyperbolic sine is defined in (2.13),

$$\frac{D(y)}{R} = \frac{H_0\tau_0}{\hat{R}} \int_y^1 \frac{\mathrm{d}\tilde{y}}{a(\tilde{y})}. \tag{6.30}$$

As for the constant $H_0\tau_0$, we refer to (2.8) and (3.11). Finally, the scale factor $g(y)$ is assembled as, see (6.2) and (6.9),

$$g(y) = \frac{h^{\lambda}(y)}{a^{s+1}(y)} \sinh^2 \frac{D(y)}{R}. \tag{6.31}$$

By making use of U' as stated after (5.21), we find the derivative $n(S) = -N'(S)$ of the cumulative count (6.28),

$$n(S) = 4\pi \hat{\rho}_0 \hat{R}^2 H_0 \tau_0 \frac{S^{\mu-1}}{S_c^{\mu}} \times \int_0^{\tau_1(\varepsilon)/\tau_0} \frac{\mathrm{d}y}{a(y)} h^{1+\delta}(y) g^{\mu}(y) \left(1 + g(y)\frac{S}{S_c}\right)^{\nu} \times \mathrm{e}^{-\kappa g(y) S/S_c} \sinh^2 \frac{D(y)}{R}. \tag{6.32}$$

The amplitude n_1 in (6.26) is recovered by dropping all factors depending on the S/S_c ratio as well as $\hat{\rho}_0$. The constant N_∞ in (6.13) is calculated by setting $S = 0$ in (6.28), which amounts to replacing the incomplete Kummer function U by $F(0)$, see (6.12). The exponent ξ in (6.14) has to be negative for this limit N_∞ to exist.

Since $S_c \propto 1/R^2$, see (6.9), it is convenient to replace S_c with the curvature-independent flux scale $S_0 :=$

$L_c H_0^2/(4\pi c^2)$, by substituting $S_c = S_0/\hat{R}^2$ into the above formulas. That is, we use S_0 instead of S_c as fitting parameter. The high-S scaling valid for positive exponents χ and φ (defined in (6.21) and (6.22)) reads

$$n(S\to\infty) \sim \frac{\hat{\rho}_0 n_\infty}{\hat{R}^3}\frac{S_0^{3/2}}{S^{5/2}},$$
$$N(S\to\infty) \sim \frac{2}{3}\frac{\hat{\rho}_0 n_\infty}{\hat{R}^3}\frac{S_0^{3/2}}{S^{3/2}}, \tag{6.33}$$

with amplitude n_∞ defined in (6.20). The low-S scaling (again for positive χ and φ, see the text after (6.25)) is

$$n(S\to 0) \sim \frac{\hat{\rho}_0 n_0}{\hat{R}^{2\sigma}}\frac{S_0^{\sigma}}{S^{\sigma+1}},$$
$$N(S\to 0) \sim \frac{\hat{\rho}_0 n_0}{\sigma\hat{R}^{2\sigma}}\frac{S_0^{\sigma}}{S^{\sigma}}, \tag{6.34}$$

with amplitude n_0 in (6.24). The amplitudes $n_{\infty,0}$ depend on the curvature radius $\hat{R}$. The number count pertaining to a flat 3-space is recovered by performing the limit $\hat{R}\to\infty$. In this limit, $\sinh(D/R)$ is replaced by D/R in (6.28), (6.31), and (6.32). As for the amplitude n_0 in (6.24), $\sinh D_\infty$ is replaced by D_∞, see (3.7); since $S_c = S_0/\hat{R}^2$, $\hat{R}$ drops out.

The break flux S_b in the crossover region is defined by equating the asymptotic power laws $n(S_b)$ in (6.33) and (6.34), so that $S_0 = S_b\hat{R}^2(n_0/n_\infty)^{2/(3-2\sigma)}$. The amplitudes $n_{\infty,0}$ are stated in (6.20) and (6.24). The break flux $S_{b,N}$ of the cumulative count is obtained by equating the asymptotic $N(S_{b,N})$ in (6.33) and (6.34), $S_b = S_{b,N}(2\sigma/3)^{2/(2\sigma-3)}$. In this way, we have parametrized the flux scale S_0 by the break flux of the differential or cumulative count. The asymptotic counts $N(S\to 0,\infty)$ appear as straight lines in double-logarithmic plots, intersecting at $S_{b,N}$.

In Fig. 3, we fit cumulative counts of soft X-ray point sources. To this end, we introduce dimensionless quantities, writing S_{14} for S in units of 10^{-14} erg cm^{-2} s^{-1}. We write the cumulative count in (6.33) as $N(S)\sim 2A_\infty S_{14}^{-3/2}/3$, so that $\hat{\rho}_0 = A_\infty S_{0,14}^{-3/2}\hat{R}^3/n_\infty$, which is independent of the curvature radius, since $n_\infty\propto\hat{R}^3$. The dimensionless amplitude A_∞ is customarily given per deg^2. S_{14} stands for $S/(10^{-14}$ erg cm^{-2} s$^{-1})$, and analogously $S_{0,14}$.

The fit in Fig. 3 is based on the integral representation (6.28) of the cumulative count. The expansion factor (6.29) is specified as in (3.10) and (3.11); in particular, the high-z asymptotics of the Hubble parameter is defined by the scaling exponent $n=2$, see (3.16). As for the spectral index in (6.31), we set $s=1$ in the 0.5–2 keV range considered (Cappelluti et al. 2007, 2009). The luminosity evolution is specified by the scaling exponent $\lambda=6$. The exponent of the density evolution is $\delta=0$, see the text after (5.16). As for the derived asymptotic scaling exponents, we find $\xi=1$, see (6.14), $\chi=14$, see (6.21), and $\sigma=1/14$, see (6.23); the exponent φ is positive provided that $\mu>0$, see (6.22). A positive μ is suggested by the rapid initial rise in the redshift evolution of the AGN space density, see Fig. 2 and the text after (5.15). The exponents determining the luminosity scaling function (5.3) are taken from the fit of the AGN space density in Fig. 2, $\mu=2$, $\nu=-5/2$, and $\kappa\approx 1.6\times 10^{-5}$, see the text after (5.16). Regarding the curvature radius, we set $\hat{R}=10$, which is already in the Euclidean regime according to the fit of the SN Ia distance moduli in Fig. 1, see the text after (4.10). Parameters extracted from the fit in Fig. 3 are the flux scale $S_{0,14}\approx 1.1\times 10^{-4}$, the density scale $\hat{\rho}_0\approx 8.0\times 10^3$, see (6.33) and (6.34), and the cutoff $\varepsilon\approx 0.39$ determining the emission time in the upper integration boundary of $N(S)$ in (6.28). Derived parameters (discussed above, after (6.34)) are the asymptotic amplitudes $n_0\approx 31.4$, $n_\infty\approx 3.9\times 10^8$, and $A_\infty\approx 3.5\times 10^3/\mathrm{deg}^2$, as well as the break flux $S_{b,N,14}\approx 1.19\times 10^{-2}$.

7 Conclusions

(1) In Sect. 4.2, we performed a fit of the SN Ia Hubble diagram covering redshifts up to $z\approx 1.75$. In this redshift range, the curvature radius of the 3-space enters only very weakly in the distance modulus plotted in Fig. 1, as this is still the low-z regime, where the ascending series (4.10) and (4.16) of the luminosity distance and the Hubble parameter can be employed. We found a linear scaling of the SN Ia luminosity with the normalized Hubble parameter, $L/L_0 = h(z)$, where $h(z) = H(z)/H_0 = G(z)/G_0$, see (2.4), possibly caused by a dependence of the distance modulus on host-galaxy metallicity as argued in Gallagher et al. (2008).

(2) In Sect. 5, we investigated the comoving space density $\rho\propto h^{1+\delta}(z)F(Lh^\lambda(z))$, with scaling function F in (5.3). The redshift dependence of $\rho(z,L)$ occurs exclusively via the scaling variable $h(z)$. In Fig. 2, we showed that the steep initial rise of the AGN space density can readily be fitted with this ansatz for $\rho(z,L)$ and the exponents $\delta=0$ and $\lambda=6$. The scaling function F in (5.3) models the crossover from power-law increase to power-law decay and subsequent exponential decay in the high-luminosity regime; the respective exponents μ, ν, and κ determining its overall shape are obtained from the fit in Fig. 2, see the text after (5.16).

(3) In Sect. 6, we studied flux-limited number counts. We derived the redshift scaling of the flux-parametrized luminosity function and the associated differential and cumulative counting functions, in particular, their dependence on the Hubble parameter as scaling variable, see (6.7). In Sect. 6.2, we calculated the high-flux and low-flux asymptotics of the counting functions, arriving at elementary scaling relations in these limits determined

by the scaling exponents of the AGN luminosity function and the cosmic expansion factor. In Sect. 6.3, we assembled the integral representation of the cumulative count used in the fit of the X-ray source counts in Fig. 3. A curvature radius above 4×10^4 Mpc, roughly 10 times the Hubble distance c/H_0, does not noticeably affect the fit, so that a Euclidean 3-space geometry suffices to model the counting functions.

The expansion factor, in particular the deceleration parameter used in the fits in Figs. 1–3 (see (2.6), (3.10), and (4.2)), and the associated Hubble parameter and gravitational constant (2.4) can be subjected to three other standard tests, namely, the redshift evolution of linear and angular diameters as well as the surface brightness test (Sandage 1995), which will be discussed elsewhere.

Acknowledgements The author acknowledges the support of the Japan Society for the Promotion of Science. The hospitality and stimulating atmosphere of the Centre for Nonlinear Dynamics, Bharathidasan University, Trichy, and the Institute of Mathematical Sciences, Chennai, are likewise gratefully acknowledged.

References

Amsler, C., et al.: Review of particle physics. Phys. Lett. B **667**, 1 (2008)

Babbedge, T.S.R., et al.: Luminosity functions for galaxies and quasars in the Spitzer Wide-Area Infrared Extra-galactic (SWIRE) Legacy survey. Mon. Not. R. Astron. Soc. **370**, 1159 (2006)

Baldi, A., et al.: The HELLAS2XMM Survey. I. The X-ray data and the log N–log S relation. Astrophys. J. **564**, 190 (2002)

Bauer, F.E., et al.: The fall of active galactic nuclei and the rise of star-forming galaxies: a close look at the Chandra Deep Field X-ray number counts. Astron. J. **128**, 2048 (2004)

Brunner, H., et al.: XMM-Newton observations of the Lockman Hole: X-ray source catalogue and number counts. Astron. Astrophys. **479**, 283 (2008)

Cappelluti, N., et al.: The XMM-Newton Wide-Field Survey in the COSMOS Field. II. X-ray data and the log N–log S relations. Astrophys. J. Suppl. **172**, 341 (2007)

Cappelluti, N., et al.: The XMM-Newton wide-field survey in the COSMOS field. The point-like X-ray source catalogue. Astron. Astrophys. **497**, 635 (2009)

Carrera, F.J., et al.: The XMM-Newton serendipitous survey. III. The AXIS X-ray source counts and angular clustering. Astron. Astrophys. **469**, 27 (2007)

Cowan, J.J., Sneden, C.: Heavy element synthesis in the oldest stars and the early Universe. Nature **440**, 1151 (2006)

Croom, M.S., et al.: The 2dF QSO Redshift Survey—XII. The spectroscopic catalogue and luminosity function. Mon. Not. R. Astron. Soc. **349**, 1397 (2004)

Dauphas, N.: The U/Th production ratio and the age of the Milky Way from meteorites and Galactic halo stars. Nature **435**, 1203 (2005)

Dirac, P.A.M.: A new basis for cosmology. Proc. R. Soc. (Lond.) A **165**, 199 (1938)

Dyson, F.J.: The fundamental constants and their time variation. In: Salam, A., Wigner, E.P. (eds.) Aspects of Quantum Theory. Cambridge University Press, Cambridge (1972)

Elvis, M., et al.: The Chandra COSMOS Survey, I: overview and point source catalog. Astrophys. J. Suppl. **184**, 158 (2009)

Fan, X., et al.: High-redshift quasars found in Sloan Digital Sky Survey commissioning data. III. A color-selected sample at $i^* < 20$ in the Fall Equatorial Stripe. Astron. J. **121**, 31 (2001)

Fan, X., et al.: A survey of $z > 5.7$ quasars in the Sloan Digital Sky Survey. III. Discovery of five additional quasars. Astron. J. **128**, 515 (2004)

Ferrarese, L., et al.: The Hubble Space Telescope Key Project on the extragalactic distance scale. XXVI. The calibration of Population II secondary distance indicators and the value of the Hubble constant. Astrophys. J. **529**, 745 (2000)

Gallagher, J.S., et al.: Supernovae in early-type galaxies: directly connecting age and metallicity with Type Ia luminosity. Astrophys. J. **685**, 752 (2008)

Gilli, R., Comastri, A., Hasinger, G.: The synthesis of the cosmic X-ray background in the Chandra and XMM-Newton era. Astron. Astrophys. **463**, 79 (2007)

Guenther, D.B., Krauss, L.M., Demarque, P.: Testing the constancy of the gravitational constant using helioseismology. Astrophys. J. **498**, 871 (1998)

Hasinger, G., et al.: The ROSAT Deep Survey. I. X-ray sources in the Lockman Field. Astron. Astrophys. **329**, 482 (1998)

Hasinger, G., Miyaji, T., Schmidt, M.: Luminosity-dependent evolution of soft X-ray selected AGN. New Chandra and XMM-Newton surveys. Astron. Astrophys. **441**, 417 (2005)

Jimenez, R., et al.: Constraints on the equation of state of dark energy and the Hubble constant from stellar ages and the cosmic microwave background. Astrophys. J. **593**, 622 (2003)

Kasting, J.F., Catling, D.: Evolution of a habitable planet. Annu. Rev. Astron. Astrophys. **41**, 429 (2003)

Kessler, R., et al.: First-year Sloan Digital Sky Survey-II supernova results: Hubble diagram and cosmological parameters. Astrophys. J. Suppl. **185**, 32 (2009)

Komatsu, E., et al.: Five-year Wilkinson Microwave Anisotropy Probe observations: cosmological interpretation. Astrophys. J. Suppl. **180**, 330 (2009)

Kowalski, M., et al.: Improved cosmological constraints from new, old, and combined supernova datasets. Astrophys. J. **686**, 749 (2008)

Lehmer, B.D., et al.: The Extended Chandra Deep Field-South Survey: Chandra point- source catalogs. Astrophys. J. Suppl. **161**, 21 (2005)

Magnus, W., Oberhettinger, F., Soni, R.P.: Formulas and Theorems for the Special Functions of Mathematical Physics. Springer, New York (1966)

Miyaji, T., Hasinger, G., Schmidt, M.: Soft X-ray AGN luminosity function from ROSAT surveys. II. Table of the binned soft X-ray luminosity function. Astron. Astrophys. **369**, 49 (2001)

Moretti, A., et al.: The resolved fraction of the cosmic X-ray background. Astrophys. J. **588**, 696 (2003)

Müller, J., Biskupek, L.: Variations of the gravitational constant from lunar laser ranging data. Class. Quantum Gravity **24**, 4533 (2007)

Newman, M.J., Rood, R.T.: Implications of solar evolution for the Earth's early atmosphere. Science **198**, 1035 (1977)

Percival, W.J., et al.: Baryon acoustic oscillations in the Sloan Digital Sky Survey Data Release 7 galaxy sample. Mon. Not. R. Astron. Soc. (2009). arXiv:0907.1660

Puccetti, S., et al.: The XMM-Newton survey of the ELAIS-S1 field. I. Number counts, angular correlation function and X-ray spectral properties. Astron. Astrophys. **457**, 501 (2006)

Reid, B.A., et al.: Cosmological constraints from the clustering of the Sloan Digital Sky Survey DR7 luminous red galaxies. Mon. Not. R. Astron. Soc. (2009). arXiv:0907.1659

Richards, G.T., et al.: The Sloan Digital Sky Survey quasar survey: quasar luminosity function from Data Release 3. Astron. J. **131**, 2766 (2006)

Riess, A.G., et al.: Type Ia supernova discoveries at $z > 1$ from the Hubble Space Telescope: evidence for past deceleration and constraints on dark energy evolution. Astrophys. J. **607**, 665 (2004)

Riess, A.G., et al.: New Hubble Space Telescope discoveries of Type Ia supernovae at $z \geq 1$: narrowing constraints on the early behavior of dark energy. Astrophys. J. **659**, 98 (2007)

Rosati, P., et al.: The Chandra Deep Field-South: the 1 million second exposure. Astrophys. J. **566**, 667 (2002)

Sandage, A.: Observational tests of world models. Annu. Rev. Astron. Astrophys. **26**, 561 (1988)

Sandage, A.: Practical cosmology: inventing the past. In: Binggeli, B., Buser, R. (eds.) The Deep Universe. Springer, Berlin (1995)

Sandage, A., et al.: The Hubble constant: a summary of the Hubble Space Telescope program for the luminosity calibration of Type Ia supernovae by means of Cepheids. Astrophys. J. **653**, 843 (2006)

Schatz, H., et al.: Thorium and uranium chronometers applied to CS 31082-001. Astrophys. J. **579**, 626 (2002)

Schmidt, M., Schneider, D.P., Gunn, J.E.: Spectroscopic CCD surveys for quasars at large redshift. IV. Evolution of the luminosity function from quasars detected by their Lyman-alpha emission. Astron. J. **110**, 68 (1995)

Silverman, J.D., et al.: Comoving space density of X-ray-selected active galactic nuclei. Astrophys. J. **624**, 630 (2005)

Silverman, J.D., et al.: The luminosity function of X-ray-selected active galactic nuclei: evolution of supermassive black holes at high redshift. Astrophys. J. **679**, 118 (2008)

Sneden, C., et al.: Neutron-capture element abundances in the globular cluster M15. Astrophys. J. **536**, L85 (2000)

Stritzinger, M., et al.: Constraints on the progenitor systems of Type Ia supernovae. Astron. Astrophys. **450**, 241 (2006a)

Stritzinger, M., et al.: Consistent estimates of ^{56}Ni yields for Type Ia supernovae. Astron. Astrophys. **460**, 793 (2006b)

Tomaschitz, R.: Ether, luminosity and galactic source counts. Astrophys. Space Sci. **259**, 255 (1998)

Tomaschitz, R.: Cosmic time variation of the gravitational constant. Astrophys. Space Sci. **271**, 181 (2000)

Tomaschitz, R.: Faint young Sun, planetary paleoclimates and varying fundamental constants. Int. J. Theor. Phys. **44**, 195 (2005)

Ueda, Y., et al.: Cosmological evolution of the hard X-ray active galactic nucleus luminosity function and the origin of the hard X-ray background. Astrophys. J. **598**, 886 (2003)

Ueda, Y., et al.: The Subaru/XMM-Newton Deep Survey (SXDS). III. X-ray data. Astrophys. J. Suppl. **179**, 124 (2008)

Wall, J.V., et al.: The Parkes quarter-Jansky flat-spectrum sample. III. Space density and evolution of QSOs. Astron. Astrophys. **434**, 133 (2005)

Williams, J.G., et al.: Lunar laser ranging science: gravitational physics and lunar interior and geodesy. Adv. Space Res. **37**, 67 (2006)

Wolf, C., et al.: The evolution of faint AGN between $z \approx 1$ and $z \approx 5$ from the COMBO-17 survey. Astron. Astrophys. **408**, 499 (2003)

Wood-Vasey, W.M., et al.: Observational constraints on the nature of dark energy: first cosmological results from the ESSENCE Supernova Survey. Astrophys. J. **666**, 694 (2007)